Contact Freezing of Water Droplets by Crystalline Organic Acids

Zachary R. Schiffman[1,2,3], Kyle A. McMillan[1,2], Dharma M. Johnson[1,2], Raina V. Gough[1,2], Ryan D. Davis[4,5], Sarah D. Brooks[6], and Margaret A. Tolbert[*1,2]

[1]*Cooperative Institute for Research in Environmental Sciences, University of Colorado, Boulder, Boulder, CO 80309, USA*

[2]*Department of Chemistry, University of Colorado, Boulder, Boulder, CO 80309, USA*

[3]*Department of Chemistry, University of California, Irvine, Irvine, CA92697,USA*

[4]*Sandia National Laboratories, Albuquerque, NM 87123, USA*

[5]*Department of Chemistry and Chemical Biology, University of New Mexico, Albuquerque, NM 87131, USA*

[6]*Department of Atmospheric Sciences, Texas A&M University, College Station, TX 77843, USA*

[*]Email: Tolbert@colorado.edu

KEYWORDS. Clouds; Contact Freezing; Ice; Nucleation; Organic Aerosol

ABSTRACT.

The ability of water to freeze into ice crystals in mixed-phase clouds affects physical properties including particle size, precipitation rates, and radiative properties. The presence of an insoluble particle at the surface of water droplets can promote ice nucleation at higher temperatures than pure water, even in the absence of a collision. However, contact freezing remains an underexplored mode of ice nucleation. Here, we present a study of atmospherically relevant

organic acids and their role as effective ice-nucleating particles in the contact mode using a Raman-microscope-equipped environmental chamber. We determined contact freezing temperatures induced by solid crystals of docosanol, adipic acid, cis-pinonic acid, fumaric acid, 4-hydroxybenzoic acid, palmitic acid, phthalic acid, sebacic acid, stearic acid, terephthalic acid, and vanillic acid. All solids except fumaric acid promoted contact freezing of water droplets at significantly higher temperatures than pure water in the chamber (-15.0 to -18.5 °C vs -21.3 °C). Physical and chemical properties were identified which correlate with greater effectiveness of ice-nucleating particles in the contact mode including crystal lattice mismatch with ice, carbon number, and insolubility in water. We suggest that the presence of these organic solids in atmospheric aerosol may promote atmospheric ice nucleation at warm temperatures.

SYNOPSIS.

Contact freezing may be a crucial contributor to atmospheric ice nucleation, but the chemical and physical mechanism and fundamental characteristics of contact ice nucleating have not yet been established. Here, several organic solids are reported which significantly increase the freezing temperature of water when in contact with the droplet.

TOC GRAPHIC

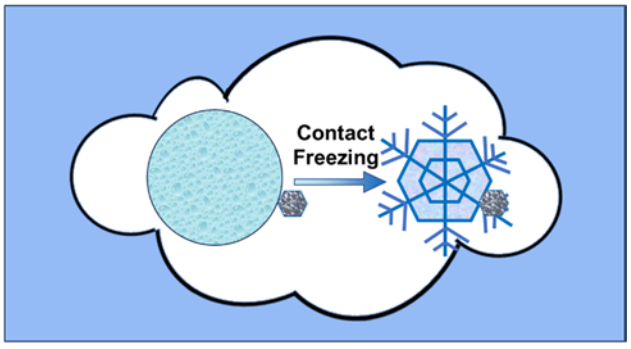

1. Introduction

Ice crystals in mixed-phase clouds play a significant role in the global radiative balance, contributing to both warming and cooling effects on climate.[1–6] The ratio of liquid water to ice in these clouds impacts their physical properties including particle size, shape, and precipitation rates, which in turn influence their absorption and scattering properties.[7–17] However, the ice nucleation mechanism in mixed-phase clouds is uncertain, and further research is needed to constrain the atmospheric impacts of this crystalline solid. Pure water droplets, when unperturbed, freeze at approximately -38°C,[17] although the exact freezing temperature depends on factors including relative humidity, solute concentrations, and droplet size.[18–21] In contrast, the presence of insoluble particles in atmospheric aerosol can promote heterogeneous ice nucleation, causing freezing at higher temperatures or lower water saturation levels than would be required homogeneously.[13,22] These particles promote ice formation by providing a stable surface and lowering the energy barrier to crystal nucleation.[23] These effects likely influence the characteristics of ice particles in mixed-phase clouds, including their number and size.[24]

There are several possible modes by which heterogeneous freezing can occur, as displayed in Figure 1 following descriptions by Kanji et al.[17] Deposition freezing occurs when ice deposits onto a heterogeneous particle from supersaturated water vapor. This mode requires low temperatures and is likely not a major nucleation mechanism in tropospheric mixed-phase clouds.[25] Immersion freezing derives from an insoluble particle immersed inside of a droplet. In contrast, contact freezing occurs when an ice-nucleating particle (INP) touches the external surface of a water

droplet, leading to enhanced nucleation. In contact freezing, there is a three-phase contact line between the liquid water, the contact nucleus, and the surrounding air, which lowers the free-energy barrier for nucleation according to classical nucleation theory.[26] Out of all modes of heterogeneous ice nucleation, contact freezing is thought to be generally the most effective at the highest temperatures, although this depends on the INP.[27,28] Previous studies have typically involved insoluble particles, although contact freezing has also been observed for soluble salts.[29] Previous work has shown that heterogeneous freezing can occur through contact when, even in the absence of a collision event.[30–34] As defined by Marcolli et al., we define contact freezing as any freezing event in which the INP touching a droplet surface leads to enhancement of INP ability, including but not limited to "collisional contact freezing" in which the collision of the INP with the droplet leads to freezing.[35] The present study probes such static contact freezing without collision. There is evidence that collisions may create additional transient surface interactions that can further promote nucleation,[36,37] deserving further investigation beyond the scope of this study. Observational field studies have suggested that contact freezing likely leads to the first formation of ice in mixed-phase clouds, especially at the edges of low altitude clouds.[2,3,38] Ansmann et al. and Seifert et al. found that contact freezing was likely responsible for ice nucleation from dust particles and volcanic ash particles, respectively.[39,40]

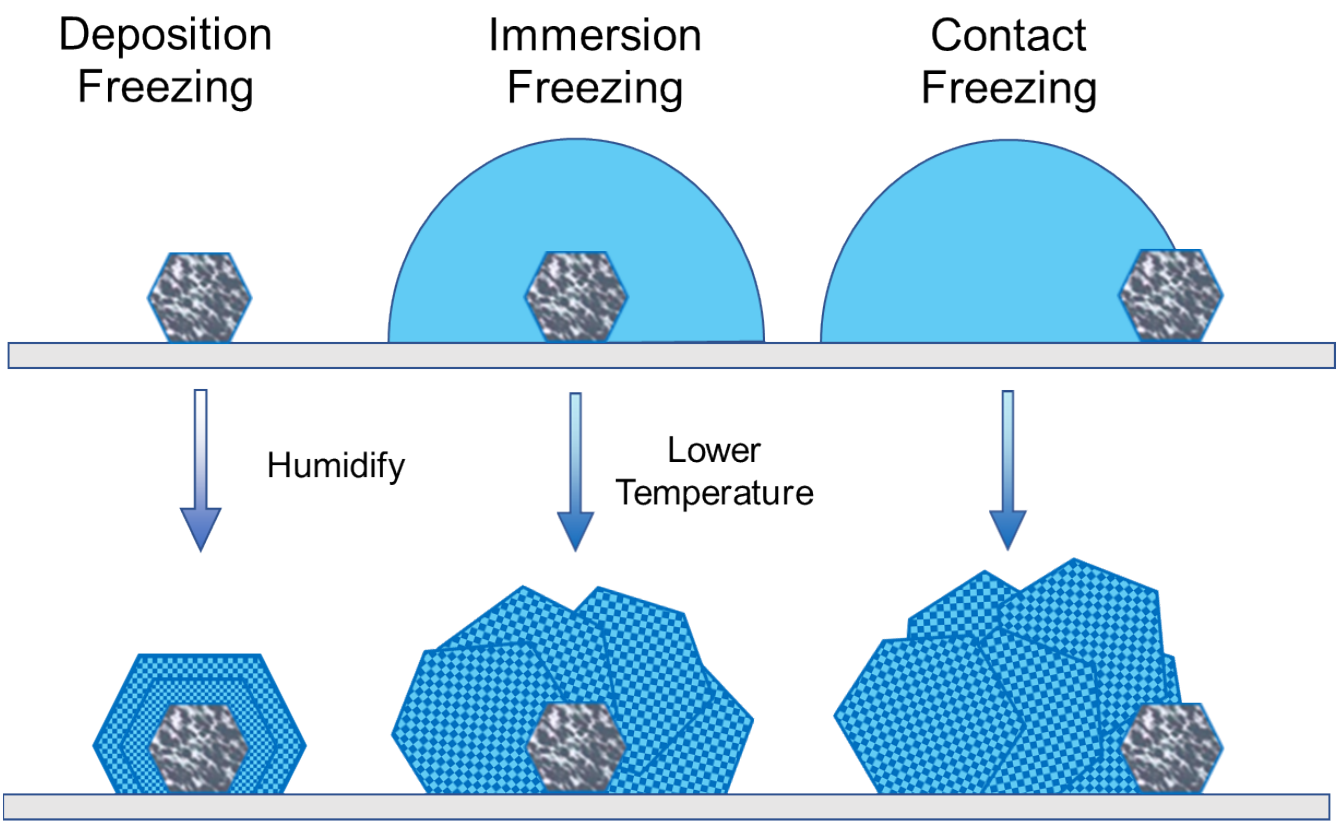

Figure 1. Diagrams of the forms of heterogeneous freezing discussed here. In deposition freezing, water vapor deposits onto the nucleus as solid ice. In immersion freezing, the insoluble nucleus is internally mixed within the liquid droplet. In contact freezing, there is a three-phase contact line between the liquid water, the insoluble contact nucleus, and the surrounding air.

Studies of atmospheric ice residuals reveal that the most common heterogeneous INPs, irrespective of freezing mode, include mineral dust, ash, metallic particles, and organics.[21,41] These INPs have been studied experimentally in deposition and immersion mode freezing, including mineral dusts and clays[31,37,42–54], soot,[31,55,56] and volcanic ash.[31,57,58] Biological particles have also been studied as INPs including microscopic organisms such as fungi,[59] phytoplankton,[60], and pollen[61] as well as isolated proteins like RuBisCO[62] and inaZ (i.e., SnoMax®).[63,64] In addition, it has long been suggested that certain organic compounds in atmospheric particles, both from anthropogenic and from natural origin, can act as INPs, dependent on the freezing mechanism.[65–

[68] Organic compounds make up a significant fraction of residuals left behind after the melting of atmospheric ice crystals.[69–71] However, observations show that only certain particulate organics are capable of nucleating ice. Although a few studies have explored contact ice nucleation by organic solids and even some viscous liquids,[32,33,72,73] there is still a lack of experimental data in this area as well as relevant theory regarding which organics are the most effectives INPs in this mode.

Here, we study contact freezing of water droplets by atmospherically relevant, oxygen-containing organic solids in an environmental chamber equipped with Raman microscopy capabilities. We combine visual observations with Raman data to determine the contact freezing temperatures. We then compare these results to freezing of pure water as well as contact freezing by crystalline silver iodide, a well-known and highly effective ice nucleus. We consider physical properties of the organic solids in an attempt to uncover correlations among the freezing temperatures, identify potential trends, and contextualize the results within previous literature.

2. Experimental Methods

2.1. Raman Microscope and Environmental Chamber

The Raman microscope and environmental chamber, shown schematically in Figure 2, have been used previously to study ice nucleation in the deposition mode[74–78] and the immersion mode.[76] Here, modifications in the method will be described to allow for the study of contact ice nucleation. A prepared quartz slide was placed onto an iridium-coated steel block inside an environmental chamber at room temperature, which was subsequently sealed. The relative humidity inside the cell was controlled by combining flows of dry and humidified nitrogen gas in select ratios. These flows were held steady to produce consistent water content inside the cell. The

dew point was read by a chilled mirror hygrometer (Buck Research Instruments CR-1A). The dew point in experiments was set to approximately -10°C to prevent droplet evaporation from undersaturated conditions during freezing experiments. According to equations from Buck and from Marti and Mauersberger,[79,80] this dew point corresponds to ice saturation values between 1.58 and 2.78 for temperatures between -15.0 and -21.0°C. The sample temperature was controlled by balancing liquid nitrogen cooling with resistive heating and read by the temperature controller (Linkam TMS94). The measured temperature was calibrated to the actual temperature in the cell as discussed in Baustian et al.[75] and is discussed in detail in the Supporting Information (Figures S1 and S2).[79,81,82]

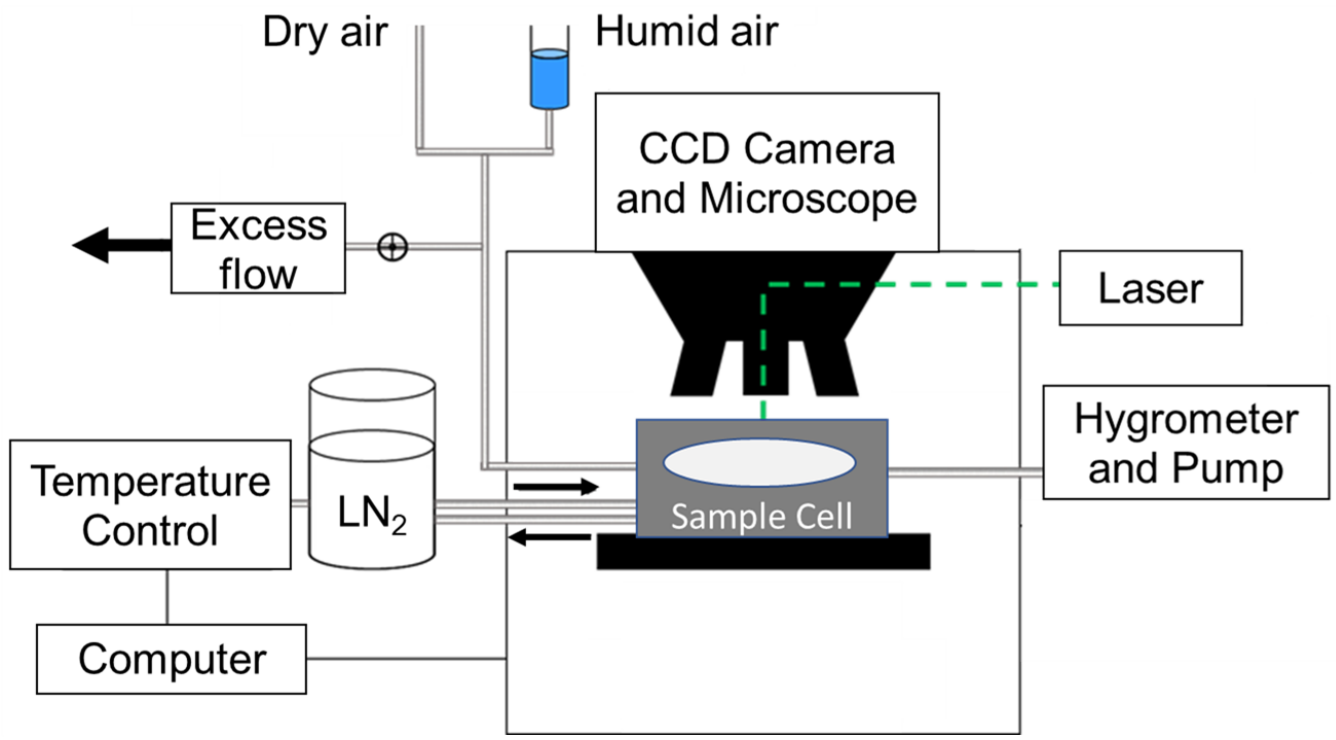

Figure 2. Instrumental schematic of Raman microscope and environmental chamber. Adapted from Schiffman et al.[37] Copyright 2023 American Chemical Society.

Raman spectroscopy was used along with visual analysis to determine the phase of the water droplet at each temperature. Raman spectra were obtained using a Nicolet Almega XR Dispersive Raman spectrometer with an 8 mW 532 nm laser to probe samples. The OH-stretching band in the Raman spectrum of water shifts to lower wavenumbers upon freezing due to the formation of hydrogen bonds between water molecules in the ice structure.[83] The Raman spectrometer was coupled with an Olympus BX51 optical microscope where particles were probed visually using a 10X magnification objective. The particles became significantly darker in the microscope images after freezing.

2.2. Materials

Table 1 lists the organic solids used in this study. In the Supporting Information (Table S1) we list the suppliers and purities of materials used here. The solids were used as they were provided with no further purification or recrystallization. The selected solid organics had low solubility in water at room temperature and at 0°C so that the heterogeneous INP could be placed in contact with the water droplet without mixing. The organic solids possessed a range of physical and chemical properties including molecular weight and solubility in water. Here we report the room-temperature and 0°C solubility of the organic solids.

Table 1. Selected chemical and physical properties of chemicals used in this study.

Chemical	Chemical Formula	Molecular Weight (g/mol)	Solubility at 25°C (g/L)	Solubility at 0°C (g/L)
Docosanol	$C_{22}H_{46}O$	326.61	$1.96*10^{-5}$ [a]	—
Adipic Acid	$C_6H_{10}O_4$	146.14	24.3[b]	7.94 [b]
Cis-Pinonic Acid	$C_{10}H_{16}O_3$	184.23	6.66 [b]	3.69 [b]
Fumaric Acid	$C_4H_4O_4$	116.07	7.0 [b]	2.30 [b]

4-Hydroxybenzoic Acid (4-HBA)	$C_7H_6O_3$	138.12	4.58 [b]	2.49 [b]
Palmitic Acid	$C_{16}H_{32}O_2$	256.42	$6.87*10^{-4}$ [b]	0.00460 [b]
Phthalic Acid	$C_8H_6O_4$	166.13	6.98 [b]	2.30 [b]
Sebacic Acid	$C_{10}H_{18}O_4$	202.25	0.247 [c]	0.0400 [b]
Stearic Acid	$C_{18}H_{36}O_2$	284.47	$5.97*10^{-4}$ [b]	0.00180 [b]
Terephthalic Acid	$C_8H_6O_4$	166.13	0.017 [d]	0.0426 [e]
Vanillic Acid	$C_8H_8O_4$	168.15	1.49[f]	1.0172 [e]

[a] Sourced from Alfa Aesar catalog. Docosanol has no published solubility data at 0°C.
[b] Sourced from the Handbook of Aqueous Solubility Data.[84]
[c] Sourced from Bretti et al. as $10^{-2.91245}$ mol/L.[85]
[d] Sourced from Park and Sheehan.[86]
[e] Experimentally determined for this study.
[f] Sourced from Zhang et al. as $1.60*10^{-2}$ mol %.[87]

Organic solids were transferred to quartz microscope slides using the end of a glass Pasteur pipet. Visual analysis of the samples on the slides suggested that the solids were crystalline particles (Figure 3). Raman spectra for the organic solids are shown in Figure S3. The experimental spectra obtained here align with previously published spectra, confirming their reliability and chemical quality.[88–97] In addition, for all the organic solids studied here, there was no overlap in spectral features in the range of the water O-H stretch that could confound the distinction between liquid water and crystalline ice.

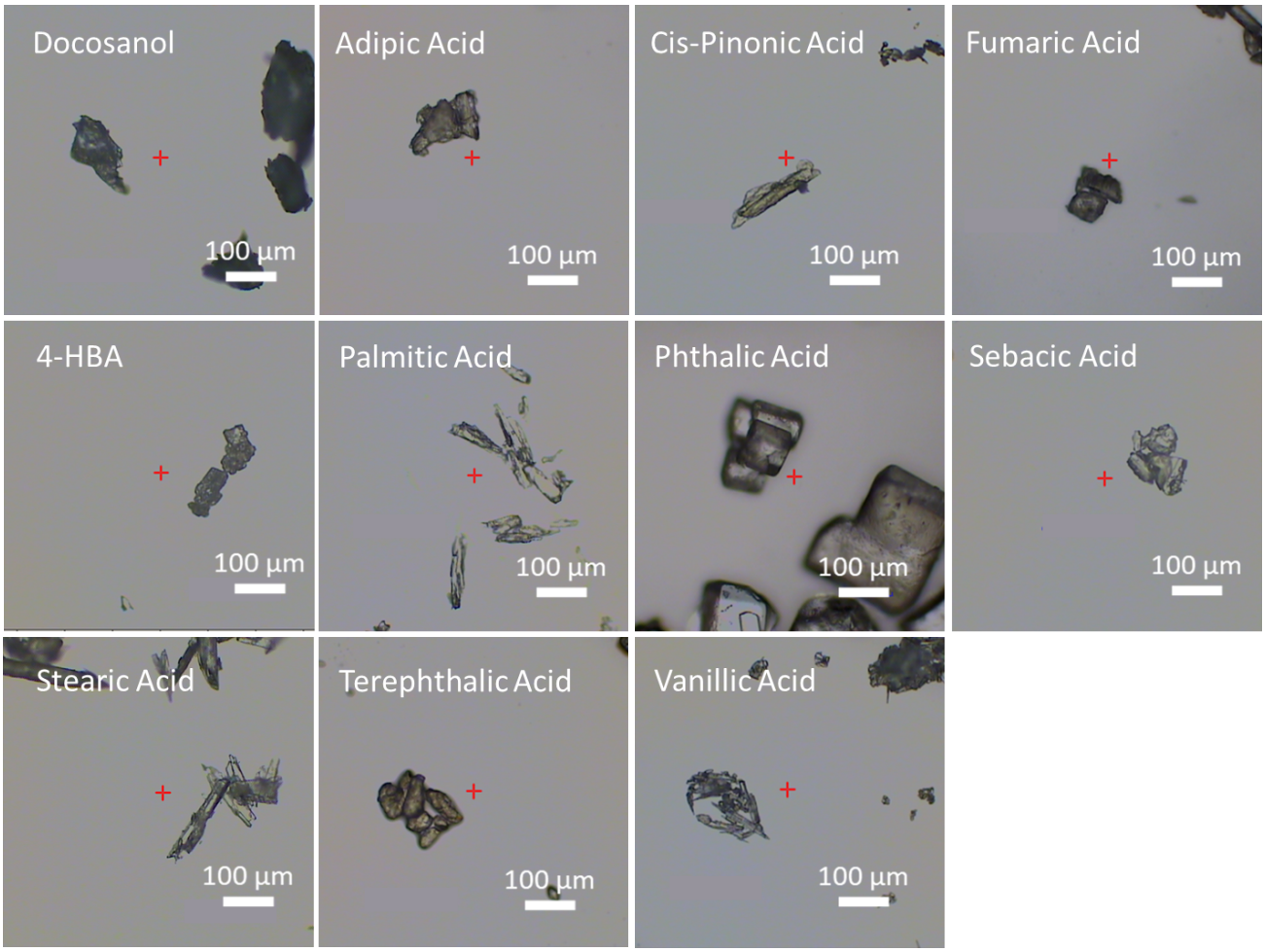

Figure 3. Microscope images of the crystalline organic solids studied here in ambient air at room temperature (~25 °C, RH ~ 40%).

In addition to microscope images and Raman spectra, the organic solids were structurally characterized using a Rigaku Ultima III X-ray Diffractometer. The diffraction peaks observed confirm that these solids are in the crystalline phase, as opposed to amorphous or glassy solids (Figure S4).[98]

2.3. Experimental Protocol for Measuring Contact Freezing Temperatures

The technique of contact freezing used here was adapted from the method of Fornea et al. and Collier and Brooks.[31,33] Using this method, we are able to disregard effects from collision rates and collision efficiency in free-floating droplets and particles and focus on phase-phase interactions.[28]

Ultra-pure water was filtered through a 0.45 μm cellulose acetate filter before use to remove microscopic particulate impurities which could act as potential INPs. Before each experiment, a quartz microscope slide was rinsed with filtered ultra-pure water and isopropyl alcohol before being treated with Rain-X® water repellent to create a quasi-hydrophobic surface. A micro-autopipette (I^2S Integrapette) was used to place a 1.0 μL droplet of filtered ultra-pure water onto the slide. Similar contact nucleation experiments performed by Fornea et al. varied the water droplet volume between 0.5 and 2.0 μL and found no significant change in freezing temperatures across the range of sizes.[31] The droplet size was calculated using the microscope image of a droplet as demonstrated in Figure S5, resulting in a radius of 650 μm, a height of 910 μm, and a contact angle of 110°.

Using a clean pipette tip, single grains of each potential heterogeneous INP were maneuvered to be in contact with the water droplet. While not explicitly controlled for size effects, particle grains were selected between approximately 250 and 450 μm in length.

During a freezing experiment the dew point was set to approximately -10°C and the temperature was set to 0°C. The temperature was lowered in increments of 0.5°C, at a cooling rate of 1°C/min in between increments. At each step, a Raman spectrum and a visual image of the droplet were obtained. Raman spectra were averages of 32 scans at a rate of 1 second per scan. Temperature was lowered in this fashion until a freezing event occurred and crystalline ice could be confirmed via both optical imagery and Raman spectroscopy. The temperature was then raised

to 5.0°C for at least three minutes until the ice crystal fully melted into liquid water, also confirmed by both optical imagery and Raman spectroscopy, at which point the cooling process was repeated. Each experiment consisted of at least five freeze-melt cycles. The melting of water occurred at 0.0°C in all experiments, indicating the accuracy of the temperature calibration performed for the environmental chamber.

We attempted two methods to conduct immersion mode ice nucleation experiments for comparison. The first method was to place 1.0 μL of filtered water directly onto a dry particle on a slide. The second method was to place 0.5 μL on either side of the particle and allow the two droplets to coalesce. This method has been used successfully to study immersion freezing of other INPs including silver iodide (manuscript in preparation). In both methods, each organic solid immediately moved through the water to the surface of the droplet and thus it was not possible to immerse the organic particle inside the droplet without contacting the droplet surface (Figure S6). This occurred for each organic solid studied spanning a range of sizes between 120 and 370 μm. As such, we conclude that for these organic solids under our experimental conditions, it was not possible to probe immersion ice nucleation.

In order to examine whether organic acids partitioning to the aqueous phase could impact the freezing of these water droplets, we dissolved select acids with the greatest solubilities (adipic and fumaric) to their saturation limits at room temperature, filtered out any remaining solid, and attempted freezing experiments of the supernatant with no solid INP. In both cases of adipic and fumaric acids, the freezing temperature was indistinguishable from pure water. As a result, we do not believe any meaningful change in ice nucleation is occurring with these systems due to dissolution.

3. Results and Discussion

3.1. Water Controls and Contact Freezing by Silver Iodide

To set benchmarks for contact freezing performed by organic solids, freezing experiments were first performed with pure water and with silver iodide as a contact INP. As discussed in Section 1, an effective heterogeneous INP will freeze water at temperatures higher than would occur with pure water.

Figure 4 shows example data for pure water freezing under our experimental conditions. The Raman peaks between 3390 and 3410 cm^{-1} were used as markers for liquid water while the peaks between 3135 and 3160 cm^{-1} indicated ice. These peak assignments agree with literature values for water and ice.[83] In addition to the Raman spectra, visual microscope images were used to confirm the phase of water as solid or liquid. The experiment began with liquid water as indicated in the top panels in Figure 4, both by visual inspection and the Raman spectrum. The temperature was then lowered and the wavenumber of maximum intensity remained in the liquid water range. Freezing was determined as a steep transition to 3140 cm^{-1} as well as darkening of the image. The freezing temperature for each cycle was selected as the calibrated temperature set by the Linkam controller where the transition from liquid to solid occurred. The temperature was then gradually increased until a melting event occurred at 0°C, as indicated by a sharp rise in

wavenumber of the peak of highest intensity to 3400 cm^{-1}. Raman spectra were obtained at the center of the red crosshair shown in the microscope images.

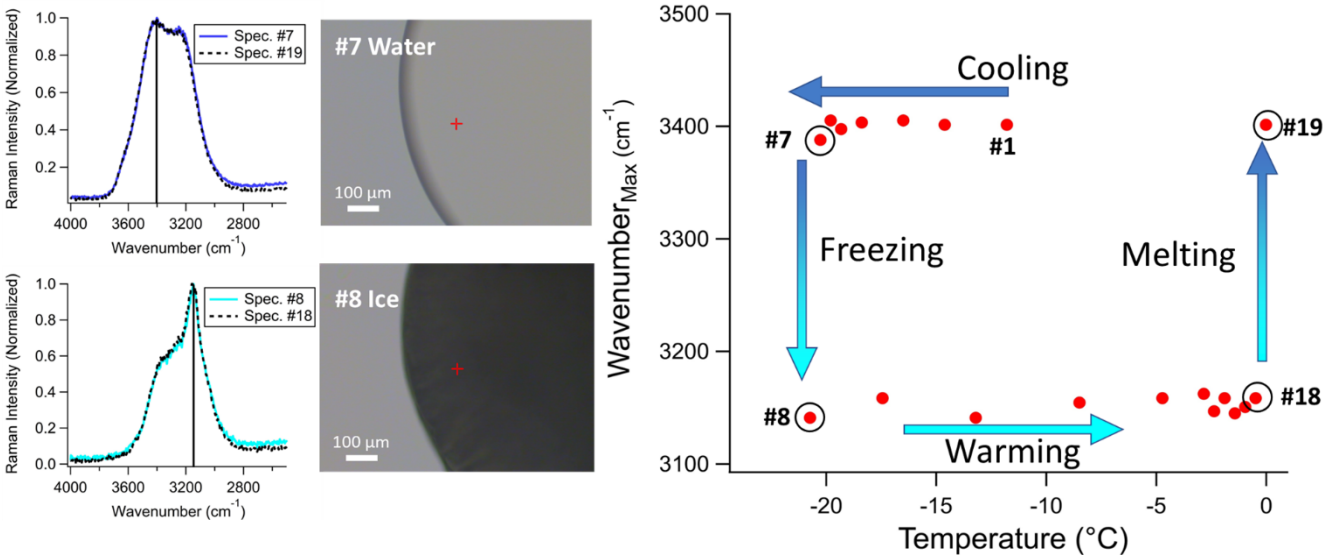

Figure 4. (Left) Raman spectra of a water droplet in the liquid phase **(top, points #7 and #19)** and crystalline phase **(bottom, points #8 and #18).** The vertical black lines indicate the wavenumber of maximum Raman intensity. **(Middle)** Microscope images of the same water droplet before freezing **(top #7, -20.2 °C)** and after freezing **(bottom, #8, -20.7 °C).** The dew point was approximately -10 °C. The red crosshair indicates where the Raman spectra were obtained. The scale bar represents a length of 100 µm. **(Right)** A plot of wavenumber of maximum Raman intensity vs temperature over the course of an experiment, which displays a hysteresis of water freezing and melting. The experiment begins at data point #1 and subsequent data points follow the directions of the arrows as indicated. The circled points correspond to the Raman spectra and microscope images presented. The determined contact freezing temperature for this experiment is -20.7°C.

The same method was employed with a contact INP of silver iodide and the determination is shown in Figure 5. As the temperature is lowered, the shift in wavenumber of maximum intensity from liquid water to solid ice occurs at significantly warmer temperatures than with pure water. However, melting occurs at the same temperature, 0°C, regardless of freezing method.

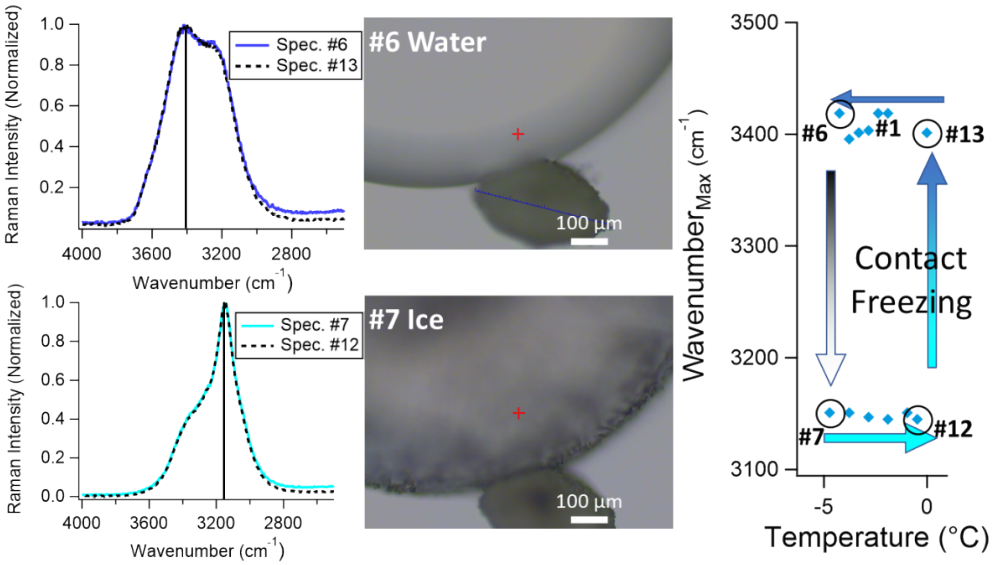

Figure 5. (Left) Raman spectra of a water droplet in contact with silver iodide in the liquid phase **(top, points #6 and #13)** and crystalline phase **(bottom, points #6 and #13).** The vertical black lines indicate the wavenumber of maximum Raman intensity. **(Middle)** Microscope images of the same water droplet before freezing **(top, #6, -4.2 °C)** and after freezing **(bottom, #7, -4.7 °C)** The dew point was approximately -10 °C. in contact with silver iodide. The grain shown has a diameter of approximately 380 µm, as measured by the thin blue line. The red crosshair indicates where the Raman spectra were obtained. The scale bar represents a length of 100 µm. **(Right)** A plot of wavenumber of maximum Raman intensity vs temperature over the course of an experiment, which displays a hysteresis of water freezing and melting. The experiment begins at data point #1 and subsequent data points follow the directions of the arrows as indicated. The circled points correspond to the Raman spectra and microscope images presented. The determined contact freezing temperature for this experiment is -4.7°C.

For each experiment, the freeze-melt cycle is repeated several times. Due to the stochastic nature of freezing events, some variance in heterogeneous freezing temperatures is to be expected.[33,49,99] As such, uncertainty is reported for each mean freezing temperature as the standard deviation of measurements. The random variation in freezing temperatures for each organic solid can be observed across all trials (Table S2). The uncertainties of measurements in this study lie within or less than the range of uncertainties reported by other studies using similar experimental methods which had greater numbers of freezing trials.[31,33] For example, when testing the freezing

temperature for pure water, the ten data points produced a mean freezing temperature of -21.3 ± 1.7°C (Figure 6). This temperature is warmer than that which would be expected from a pure water droplet in the atmosphere freezing homogeneously, which would be approximately -33°C for a droplet of comparable volume.[18] Although Fornea et al. observed freezing in pure water droplets at approximately -33°C in a similar experimental apparatus, it is possible that we are witnessing the effects of either a less hydrophobic microscope slide facilitating nucleation or contaminants in the water droplet.[31] For example, Bogler and Borduas-Dedekind reported that the use of cellulose acetate filters led to greater background freezing temperatures compared to their other filters.[100] As such, acetate leaching from the filter membranes into the water may be a source of contamination. However, because these filters still decrease background freezing relative to unfiltered water in our experiments, their use still provided a control with which to compare our organic solids' INP capabilities. Filtering pure water through 0.45 μm nylon filters did not result in a significantly different freezing temperature compared to using cellulose acetate filters. Nonetheless, we treat this pure water experiment as a baseline with which to compare our organic solids' INP capabilities. The melt-freeze cycles with silver iodide in this study produced a mean

heterogeneous freezing temperature of -5.4 ± 1.1°C, well above the values for pure water as shown in Figure 6.

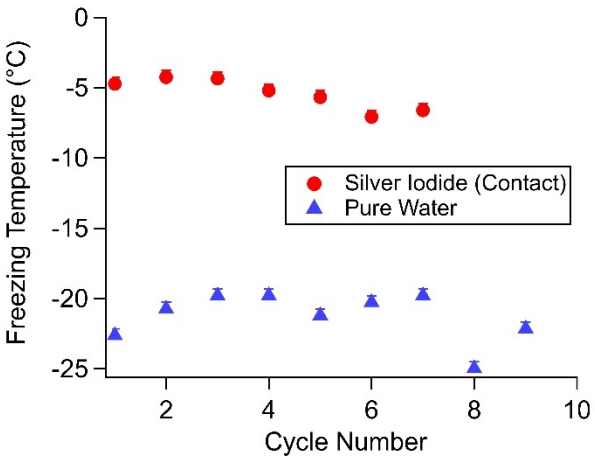

Figure 6. An example of the data sets collected throughout the pure water droplet experiment and the contact freezing experiment with silver iodide. The Linkam temperature controller measures to within ±0.1°C, setting the lower bound of error bars for freezing temperature. The Raman spectra were obtained by lowering in steps of 0.5°C, setting the upper bound of error bars. The ten data points for pure water produce a freezing temperature of -21.3 ± 1.7°C (blue triangles). The seven data points for silver iodide produce a contact freezing temperature of -5.4 ± 1.1°C (red circles).

Ice nucleation by silver iodide (AgI), a highly effective INP in both the immersion and contact modes, has been studied extensively and has been utilized in artificial snowmaking.[35] DeMott found that AgI in aerosol act as efficient contact INPs in a dynamic cloud chamber at temperatures as warm as -6°C.[101] A more recent review by Marcolli et al. of the INP ability of silver iodide reports several studies that suggest ice nucleation through contact with AgI at temperatures between -5 and -6°C, approximately 10°C warmer than when silver iodide is immersed inside the bulk of the droplet.[35] Our experimental values for contact freezing of ice by AgI are in excellent agreement with literature values. From this we conclude that a collisional

event is not necessary nor solely responsible for the enhancement of freezing ability from AgI. We thus used this technique to probe contact freezing using a range of organic acids.

3.2. Contact Freezing by Solid Organic Acids and Docosanol

The freeze-melt cycle was performed with each of the organic acids in contact with a 1.0 μL water droplet in the environmental chamber and the results are summarized in Table 2. An example of the procedure used for the organic solids as contact INPs is demonstrated with adipic acid in Figure S7. As above with pure water and silver iodide, Raman spectra were obtained as the temperature was lowered approaching the contact freezing point. For each organic, we report the recorded freezing temperature for each trial in Table S2 as well as the crystal length of each organic solid used in this study. Images of each of the other organic acids are shown in Figures S8 and S9. The organic solids remained at the droplet contact line before and after freezing (Figure S9). In addition to organic acids, the long-chain alcohol docosanol was also investigated. Docosanol has been shown to be an effective ice nucleator when coated on the surface of water droplets,[63,73] more effective than organic acids, so it acted as a point of reference compared to the organic acids.

Table 2. Mean contact freezing temperatures induced by each insoluble organic solid as determined in this study.

Organic Solid	Mean Freezing Temperature[a] (°C)
Docosanol	-15.0 ± 1.5
Palmitic	-15.6 ± 0.7
Stearic	-15.8 ± 0.7
Terephthalic	-16.5 ± 0.9
Cis-Pinonic	-16.7 ± 1.9
4-HBA	-17.1 ± 1.5

Sebacic	-17.7 ± 1.0
Phthalic	-17.9 ± 0.5
Vanillic	-18.3 ± 0.2
Adipic	-18.5 ± 0.8
Fumaric	-20.8 ± 1.7
Pure Water	-21.3 ± 1.7

[a] Uncertainty presented is the sample standard deviation across all melt-freeze cycles for each heterogeneous INP.

For each of the organic solids, statistical analysis was performed comparing the mean contact freezing temperature induced by each INP with that of pure water to determine whether the contact nucleation event occurred at a statistically higher temperature. The analysis is detailed in the Supporting Information (Table S3).[102] We found that, with 99% confidence, all but one of the organic solids studied here nucleate ice at a meaningfully higher temperature than pure water. Only fumaric acid cannot be statically distinguished as nucleating ice at a warmer temperature than pure water within this confidence.

3.3. Identifying Potential Trends in Contact Ice Nucleation Ability

To identify potential trends among contact freezing temperatures within this data set, we examine several physical and chemical parameters of the organic solids. The crystal lattice mismatch between a heterogeneous INP and ice, first described by Turnbull and Vonnegut, is considered to be potentially important to INP ability.[103] For example, it may help to explain why silver iodide is such an effective INP.[35,104] Other forms of heterogeneous crystallization phase-change events, including contact efflorescence of aqueous droplets, also appear to be promoted by a low lattice mismatch.[105,106] This phenomenon was recently shown by McMillan et al., comparing

the effectiveness of stearic and cis-pinonic acids toward contact efflorescence based on their lattice match with ammonium sulfate.[107] However, as explained by Fitzner et al., while a low mismatch with ice may promote ice nucleation, no direct correlation has been reported between heterogeneous ice nucleation and lattice match.[108,109] To investigate this relationship, we calculate the crystal lattice mismatch parameters between ice and the organic solids (Table S4).[105,110–123] Here, the lattice mismatch is defined based on the work of Davis et al. as the minimum of the following formula:

$$= \frac{\left(\left|\frac{(a_{1,INP} - a_{1,i})}{a_{1,i}}\right| + \left|\frac{(a_{2,INP} - a_{2,i})}{a_{2,i}}\right|\right)}{2},$$

where a1 and a2 are the lattice constants a, b, or c, from Table S4 defining the parameters for the INP and the ice crystal (i).[105,110] Each lattice constant of ice (a, b, and c) was compared to each constant of the INP, and the lowest calculated value is used. The organic solids used in this study have been confirmed to be in crystalline form by X-ray diffraction as shown in Figure S4.

The mean contact freezing temperatures are plotted against crystal lattice mismatch with ice in Figure 7a. Among the organic solids studied, docosanol, which has the lowest lattice mismatch, promotes the highest contact freezing temperature. However, no clear trend emerges between crystal lattice mismatch and contact freezing temperatures. Adipic acid, for example, has a relatively low lattice mismatch of 0.070 but is not an effective ice nucleator. This implies that lattice mismatch is not a reliable predictor of freezing behavior for these organic solids. This agrees with recent findings that ice nucleation does not rigorously depend on crystal lattice match.

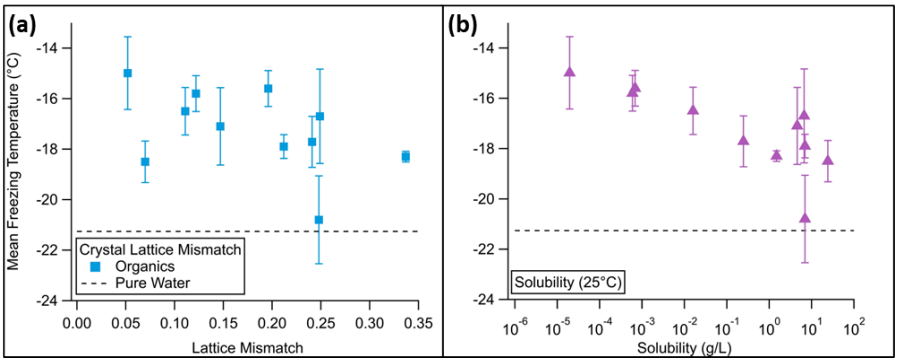

Figure 7. (a) The mean contact freezing temperatures of water from each organic solid plotted as a function of each solid's crystal lattice mismatch with ice. **(b)** Contact freezing temperatures plotted as a function of each solid's solubility in water at 25°C. The black dashed line represents the mean freezing temperature of pure water in this study. Errors bars represent sample standard deviations for each solid.

In looking for other trends, it has been found previously that films of long-chain organics on water droplets nucleate ice more efficiently than shorter-chain counterparts.[124–129] The cause of this has been attributed by some to the ability of long-chain organics to form a well-packed surface, which is crystalline and immobile in nature, onto which ice can nucleate even at high temperatures.[124–126] Molecular simulations by Qiu et al. further support that long carbon chains allow for the rigidity required for the formation of a hydrogen bonding network which leads to freezing.[128]

Others suggest that it is the flexibility of long-chain organic films, and therefore their ability to self-assemble and withstand strain, which contributes to their effectiveness as ice nuclei.[127,129] Because odd-numbered long-chain alcohols nucleate ice more effectively than even-chain counterparts, Pharoah et al. hypothesize that reduced rigidity allows for better alignment of

C–O bonds in an orientation more compatible with ice nucleation.[129] This trend relating INP ability to molecular flexibility of hydrogen-bonding groups has also been observed in other systems and modes of freezing, for example theoretically by aluminum kaolinite surfaces in the contact mode by Zielke et al.[130] or experimentally for organic crystals in the deposition mode by Fukuta and Mason.[66,131]

The interplay of necessary rigidity and flexibility helps to explain why the crystal lattice mismatches calculated from constants in Table S4 may not fully describe nucleation ability at the droplet's surface, as some substances may be more or less able to adopt a configuration which promotes ice formation. The ice nucleation temperature as a function of carbon number for the organic solids studied here is shown in Figure S10. It can be seen that among our organic solids, the molecules with higher carbon number are generally better contact INPs. This may help to explain why fumaric and adipic acids, with low carbon numbers and therefore an inability to form a rigid molecular structure, are poor contact nucleators of ice.

Moreover, there is ongoing debate about the role that hydrophilicity, the ability to bind water, plays in determining INP ability. Lupi and Molinero used molecular dynamics modeling to show that hydrophilicity does not directly predict contact nucleation ability, as different methods of increasing hydrophilicity could either increase or decrease freezing ability.[132] On one hand, molecular dynamics simulations of immersion nucleation by Cox et al. suggest that INP ability can be lost if the particle's hydrophilicity is too great.[133,134] In contrast, Brooks et al. found experimentally that oxidizing soot particles changed the particle's surface structure, increased hydrophilicity, and improved contact freezing.[32] Subsequent molecular dynamic simulations by Fitzner et al. confirm the importance of the interplay of both morphology (e.g., crystal lattice match) and hydrophilicity toward ice nucleation.[108]

An additional property to consider is partial solubility, which has been shown to detract from INP ability of organic .[28] For example, it has been found that less soluble dicarboxylic acids were the most efficient INPs in the deposition mode.[135] Mehndiratta et al. also suggest that increased solubility can disrupt the formation of critical ice nuclei and lead to decreased INP ability.[136] Simulations by Qiu et al further indicate that surface fluctuations of ice-nucleating material, including those due to solubility of the surface in water, can increase surface roughness and therefore decrease ice-nucleating ability.[128] A more soluble particle is less likely to provide a solid surface onto which ice can nucleate.

When we plot the mean contact freezing temperature induced by each organic as a function of the solid's solubility in water in Figure 7b, a moderately correlated negative logarithmic trend emerges. The two most soluble organics, adipic and fumaric acids, are the least active INPs in this study, while the least soluble organics, the fatty acids and docosanol, are the most active INPs. This appears to align with expectations that higher solubility leads to decreased freezing ability.[28,128] This trend is also parallel to our trend regarding carbon number as shown in Figure S10, as organic compounds with a longer carbon chain tend to be less soluble.[137] In Figure S11, we display the same plot with solubility in water at 0°C, which largely follows the same trend as at room temperature.

3.4. Comparison with Literature Studies of Heterogeneous Freezing of Organics

In 1966 Fukuta suggested that organic compounds which are effective INPs tend to possess polar or hydrogen-bonding groups while remaining poorly soluble in water, and tend to be crystalline solids.[66] Amphiphilic organic compounds such as long-chain alcohols, dicarboxylic

acids, and fatty acids have been studied as effective INPs in the deposition mode,[65,74,75,135,138] the immersion mode,[136,139] and in films on water droplets.[73,124,125,128,140,141] Additionally, secondary organic aerosol, which are common components of atmospheric aerosol,[142–145] have been shown to effectively promote ice nucleation in both the deposition mode[78,146–151] and the immersion mode.[77,147,148,151,152] Lohmann posits that contact freezing following anthropogenic emissions of insoluble, carbon-containing aerosol could cause a significant effect in ice clouds.[153]

Several of the organic solids investigated in the present study have been studied in other modes of heterogeneous freezing. Previous results for deposition freezing are summarized in Table S5.[65,74,135,138] An early study reported that phthalic and terephthalic acids were especially effective INP for deposition freezing at temperatures above -10°C, as well as 4-HBA and adipic acid.[65] However, that study from 1961 did not reveal the partial pressure of water vapor used, and as such it is difficult to conclude what mode of freezing actually took place. Marcolli argued that the observed freezing in these cases is more likely explained by condensation and subsequent freezing of liquid water rather than direct deposition.[17,154] Most studies show that deposition freezing typically requires low temperatures below the homogeneous freezing temperature of pure water and therefore are concluded not to be an important atmospheric process for warmer mixed-phase clouds.[25] We then must investigate other forms of heterogeneous freezing that may occur at higher temperatures.

An early study by Fletcher investigated over 1000 organic compounds in the contact nucleation mode, including several of the organic solids investigated in this study.[72] Like in this study, Fletcher placed droplets of water in contact with the organic of interest on a cold plate. However, unlike this study, Fletcher did not attempt to determine contact freezing temperature and performed all experiments at -3°C. Using this method, Fletcher concluded that adipic acid; fumaric acid; 4-

HBA; palmitic acid; phthalic acid; sebacic acid; stearic acid; and terephthalic acid were ineffective contact ice nuclei. This conclusion, however, does not account for colder temperatures that are present in actual atmospheric conditions. The contact freezing observed in the present study suggests instead that these organic compounds could in fact lead to atmospheric ice nucleation events through the contact mode at lower temperatures.

Collier and Brooks experimentally determined contact freezing temperatures induced by solid octacosane and viscous liquids squalane and squalene, as well as the same three organics after oxidation by ozone.[33] The contact freezing temperatures of organic solids reported in the current study are greater than all those presented by Collier and Brooks, both before and after exposure to ozone. One possible explanation for the differences in freezing effectiveness could be that the organic solids studied here were crystalline, whereas squalane and squalene were viscous liquids and the octacosane, both fresh and oxidized, may have had amorphous qualities. Therefore, different contact freezing mechanisms may have occurred, highlighting the greater effectiveness of crystalline solids. Additionally, the organic solids studied here have innate oxidized groups throughout the crystals, rather than the surface-level oxidation on the organics as noted in FTIR-ATR surface spectra by Collier and Brooks.[33] Because flexible oxygenated functional groups have been linked with INP ability,[66] this may help to explain why the organic acids are more active as contact INP.

Table S6 presents heterogeneous freezing temperatures observed of these organic solids in previous literature studies in the contact and immersion modes, as well as in coatings on water droplets.[63,73,124,125,128,136,139,141] It should be noted that the size of water droplets ranges between these studies. In nearly all cases, the contact freezing temperatures observed in our contact freezing apparatus are higher than those of other studies, including with larger or smaller water droplets.

For example, studies by Zobrist et al. and Mehndiratta et al. report that immersion of these organic acids did not lead to significant freezing enhancement of smaller water droplets compared with a water blank.[136,139] In contrast, in this study, we found that the organic solids promote contact freezing at temperatures significantly warmer than pure water with the exception of fumaric acid. This outcome, which reveals contact freezing as more effective than immersion freezing, is a well-documented phenomenon in literature studies of INPs.[28,155–159] However, it should be noted that larger pure water droplets are known to freeze at higher temperatures than smaller droplets, and so direct comparison may be challenging.[18]

Fatty acids, including palmitic and stearic acids, and long-chain alcohols, like docosanol, have also been studied in films on the surface of liquid water. Studies by Gavish et al. and Popovitz-Biro et al. reported that monolayers of fatty acids, including stearic acid, on the surface of water drops nucleated ice between -17 and -13°C.[124,125] Our contact freezing temperatures and freezing enhancements for palmitic and stearic acids fall within this range. However, other studies report little to no freezing enhancement from coatings of palmitic or stearic acid.[73,128,141]

DeMott et al. experimentally investigated contact freezing of small water droplets (between 0.1 and 0.4 nL, i.e. four orders of magnitude smaller than our droplets) which had been condensed onto crystalline particles of palmitic and stearic acids (less than 100 μm in length).[73] They found that these fatty acids induced freezing at temperatures which were significantly warmer than pure water (respectively, -36 and -34°C vs. -37°C), concluding that these fatty acids were effective INPs in the crystalline contact mode. Similarly, the contact experiments in this present study also found that crystalline palmitic and stearic acids nucleate ice at warmer temperatures compared to pure water (respectively, -15.6 and -15.8°C vs. -21.3°C). However, the contact freezing temperatures reported here are warmer than those reported by DeMott et al., and they produce greater

enhancements in freezing temperature vs pure water. These differences in contact freezing ability may arise due to our larger water droplets (1.0 μL vs 0.1-0.4 nL) and contact particles (250-450 μm vs < 100 nm). Further, DeMott et al. used a faster cooling rate (5 °C/min) than is used in the present study (1°C/min in steps of 0.5°C), and higher cooling rates have been associated with lower reported freezing temperatures.[31]

4. Conclusions and Atmospheric Implications

There is a general lack of experimental data investigating pure organic substances in the contact freezing mode. Collier and Brooks predicted that organic compounds found in the atmosphere would exhibit approximately similar INP abilities to each other in the contact mode, based on their study of the oxidized products of squalane, squalene, and octacosane.[33] While our results also show only small variability, we do find modest trends in INP ability in the contact mode, with freezing events occurring at temperatures ranging as high as -13.2°C for docosanol and as low as -22.6°C for fumaric acid. These findings demonstrate that freezing enhancement can occur for organic solids in contact with water droplets, even in the absence of a collisional event, as is consistent with other studies on contact nucleation.[30–34] The INP ability of these organic solids appeared to be related to their physical and chemical properties, including their crystal lattice mismatch with ice, carbon number, and solubility in water. Ultimately, these properties dictate the probability of whether the INP will have a solid surface favorable for ice formation. Fumaric acid, the C4 olefin dicarbonyl, was the only compound unable to significantly increase the freezing temperature of water, possibly due to its short carbon chain and high solubility in combination with its poor lattice match with ice.

Observations of continental atmospheric aerosol in the troposphere, both urban and remote, report that a majority of aerosol mass in submicron particles – at times up to 90% - is carbonaceous and commonly includes organic acids.[142–145] The organic solids studied here are representative of those in atmospheric aerosol, and each solid has been specifically reported in observational studies. Many aromatic organic acids are found in primary emissions, such as 4-HBA and vanillic acid in wildfire smoke from biomass burning,[160,161] or terephthalic acid from plastic burning.[162] Docosanol was found to be the most abundant alkanol emitted from plant waxes.[163,164] Other acids here are formed in secondary organic aerosol. For example, adipic acid is formed from the aqueous oxidation of cyclohexene,[165] phthalic acid from the oxidation of polyaromatic hydrocarbons,[166] sebacic acid from the oxidation of unsaturated fatty acids,[167] and cis-pinonic acid from the oxidation of alpha-pinene.[168] Additionally, in sea spray aerosol, McCluskey et al. found that a large majority, nearly 80%, of marine INPs were composed of fatty acids including palmitic acid.[169] Fatty acids are shown to potentially retain their INP ability in sea spray aerosol,[141,169] which is considered a major contributor to the global population of INPs.[170] The diverse range of these organic acids in the atmosphere could have impacts on global processes of ice nucleation. While our study presented experiments of single-component organics, atmospheric particles and droplets typically contain a complex mixture of organics as well as inorganic salts. Future research should include experiments on additional pure organics and multi-component mixtures of organics, as well as mixtures of organics and salts, to better simulate atmospheric conditions. These investigations would build our understanding of INPs and help extrapolate the trends presented here to complex organic aerosol in the atmosphere.

The contact freezing temperatures measured in this study are not intended to precisely replicate atmospheric processes. The freezing of pure water droplets here on the microscope slide, with a

mean temperature of -21.3 ± 1.7°C, occurs at warmer temperatures than similarly sized, freely floating droplets in the atmosphere. Nevertheless, the observed statistical improvement of contact freezing compared to the baseline of pure water exemplifies the enhancement which can potentially be extrapolated to atmospheric settings. While this study suggests that freezing can be promoted at the surface of droplets without requiring a collisional event, further research is needed to replicate these findings in a more realistic setting with freely floating droplets. Since atmospherically relevant contact is likely to involve a collision, experimental studies are needed to be able to make accurate extrapolation. The presence of these organic solids in atmospheric aerosol and cloud droplets may play a role in ice nucleation in aerosol or mixed-cloud environments.

ASSOCIATED CONTENT

Supporting Information. The Supporting Information is available free of charge. **(.pdf file).**

Discussion of temperature calibration (Figures S1 and S2); List of sources of materials (Table S1); Raman spectra of the organic solids (Figure S3); X-ray diffraction spectra of the organic solids (Figure S4); Determination of water droplet radius (Figure S5); Microscope images after failure to immerse organic solids (Figure S6); Determination of droplet phase in contact with adipic acid (Figure S7); Contact freezing temperature data for each trial (Table S2); Microscope images of each organic solid in contact with water droplet (Figure S8); Microscope images of terephthalic acid freezing experiment before freezing and after melting (Figure S9); Discussion of statistical analysis (Table S3); Discussion of crystal lattice match (Table S4); Plot of contact freezing temperature as function of carbon number (Figure S10); Plot of contact freezing temperatures as a

function of each solid's solubility at 0°C (Figure S11); Summary of previous deposition freezing studies (Table S5); Summary of immersion, contact, and organic coating freezing studies (Table S6).

AUTHOR INFORMATION

Corresponding Author

*Margaret A. Tolbert

Department of Chemistry, University of Colorado Boulder, Boulder, Colorado 80309, United States; Cooperative Institute for Research in Environmental Science, Boulder, Colorado 80309, United States;

orcid.org/0000-0001-5730-6412; Phone: (303) 492-3179;

Email: tolbert@colorado.edu

Author Contributions

The manuscript was written by Z.R.S. with guidance, editing, and feedback from K.A.M., R.V.G, R.D.D., S.D.B., and M.A.T. Conceptualization of work was done by Z.R.S., R.D.D., S.D.B., and M.A.T. Investigation, formal analysis, and visualization were performed by Z.R.S. and D.M.J. with guidance and feedback from K.A.M., R.V.G., R.D.D., S.D.B., and M.A.T. Resources were provided by M.A.T. Methodology and software were provided by R.V.G., S.D.B., and M.A.T. Project administration and supervision were performed by R.D.D., S.D.B., and M.A.T. All authors have given approval to the final version of the manuscript.

Notes

The authors declare no competing financial interest.

ACKNOWLEDGMENTS

This material is based upon work supported by the National Science Foundation under Award No. 2346198. Any opinions, findings, and conclusions or recommendations expressed in this material are those of the authors and do not necessarily reflect the views of the National Science Foundation.

Z.R.S. thanks Katie M. Primm and Yehor Novikov for technical support using the Raman microscope and environmental chamber, and Qiyin Lin for support with X-ray diffraction measurements.

Z.R.S. acknowledges Eleanor C. Browne, Joost A. de Gouw, Dharma Johnson, Upasna B. Rai, and Kevin T. Jansen for meaningful discussions regarding methodology, results, analysis, and graphic visualization.

R.D.D. is supported by Sandia's Laboratory Directed Research and Development program (project 233045). Sandia National Laboratories is a multimission laboratory managed and operated by National Technology & Engineering Solutions of Sandia, LLC, a wholly owned subsidiary of Honeywell International Inc., for the U.S. Department of Energy's National Nuclear Security Administration under contract DE-NA0003525. This paper describes objective technical results

and analysis. Any subjective views or opinions that might be expressed in the paper do not necessarily represent the views of the U.S. Department of Energy or the United States Government.

The authors acknowledge the use of facilities and instrumentation at the UC Irvine Materials Research Institute (IMRI), which is supported in part by the National Science Foundation through the UC Irvine Materials Research Science and Engineering Center (DMR-2011967).

ABBREVIATIONS

4-HBA: 4-Hydroxybenzoic Acid

INP: Ice-nucleating particle

REFERENCES

(1) English, J. M.; Kay, J. E.; Gettelman, A.; Liu, X.; Wang, Y.; Zhang, Y.; Chepfer, H. Contributions of Clouds, Surface Albedos, and Mixed-Phase Ice Nucleation Schemes to Arctic Radiation Biases in CAM5. *J Clim* **2014**, *27* (13), 5174–5197. https://doi.org/10.1175/JCLI-D-13-00608.1.

(2) Hobbs, P. V.; Atkinson, D. G. The Concentrations of Ice Particles in Orographic Clouds and Cyclonic Storms over the Cascade Mountains. *J Atmos Sci* **1976**, *33*, 1362–1374.

(3) Hobbs, P. V.; Rangno, A. L. Ice Particle Concentrations in Clouds. *J Atmos Sci* **1985**, *42* (23), 2523–2549.

(4) Yi, B.; Yang, P.; Baum, B. A.; L'Ecuyer, T.; Oreopoulos, L.; Mlawer, E. J.; Heymsfield, A. J.; Liou, K. N. Influence of Ice Particle Surface Roughening on the Global Cloud Radiative Effect. *J Atmos Sci* **2013**, *70* (9), 2794–2807. https://doi.org/10.1175/JAS-D-13-020.1.

(5) Lawson, R. P.; Gettelman, A. Impact of Antarctic Mixed-Phase Clouds on Climate. *Proc Natl Acad Sci U S A* **2014**, *111* (51), 18156–18161. https://doi.org/10.1073/pnas.1418197111.

(6) Costa, A.; Meyer, J.; Afchine, A.; Luebke, A.; Günther, G.; Dorsey, J. R.; Gallagher, M. W.; Ehrlich, A.; Wendisch, M.; Baumgardner, D.; et al. Classification of Arctic, Midlatitude and Tropical Clouds in the Mixed-Phase Temperature Regime. *Atmos Chem Phys* **2017**, *17* (19), 12219–12238. https://doi.org/10.5194/acp-17-12219-2017.

(7) Heymsfield, A. Cirrus Uncinus Generating Cells and the Evolution of Cirriform Clouds. Part I: Aircraft Observations of the Growth of the Ice Phase. *J Atmos Sci* **1975**, *32*, 799–808.

(8) Liou, K. Influence of Cirrus Clouds on Weather and Climate Processes: A Global Perspective. *Mon Weather Rev* **1986**, *114* (6), 1167–1199.

(9) Stephens, G. L.; Tsay, S.; Stackhouse, P. W. , J. P. J. The Relevance of the Microphysical and Radiative Properties of Cirrus Clouds to Climate and Climatic Feedback. *J Atmos Sci* **1990**, *47* (14), 1742–1753.

(10) Zhao, G.; Yang, J.; Zhu, L.; Xie, Z.; Lu, C.; Yin, Y.; Jing, X.; Li, J.; Wang, Y. Liquid-Ice Mass Partitioning Across the Edge of Mixed-Phase Cumulus Clouds. *Geophys Res Lett* **2023**, *50* (23), 1–8. https://doi.org/10.1029/2023GL106378.

(11) Yang, P.; Baum, B. A.; Heymsfield, A. J.; Hu, Y. X.; Huang, H. L.; Tsay, S. C.; Ackerman, S. Single-Scattering Properties of Droxtals. *J Quant Spectrosc Radiat Transf* **2003**, *79–80*, 1159–1169. https://doi.org/10.1016/S0022-4073(02)00347-3.

(12) Warren, S. G.; Brandt, R. E. Optical Constants of Ice from the Ultraviolet to the Microwave: A Revised Compilation. *Journal of Geophysical Research Atmospheres* **2008**, *113* (D14220), 1–10. https://doi.org/10.1029/2007JD009744.

(13) Korolev, A.; McFarquhar, G.; Field, P. R.; Franklin, C.; Lawson, P.; Wang, Z.; Williams, E.; Abel, S. J.; Axisa, D.; Borrmann, S.; et al. Mixed-Phase Clouds: Progress and Challenges. *Meteorological Monographs* **2017**, *58*, 5.1-5.50. https://doi.org/10.1175/amsmonographs-d-17-0001.1.

(14) Sun, Z.; Shine, K. P. Parameterization of Ice Cloud Radiative Properties and Its Application to the Potential Climatic Importance of Mixed-Phase Clouds. *J Clim* **1995**, *8*, 1874–1888.

(15) Korolev, A.; Milbrandt, J. How Are Mixed-Phase Clouds Mixed? *Geophys Res Lett* **2022**, *49* (18), 1–7. https://doi.org/10.1029/2022GL099578.

(16) DeMott, P. J.; Prenni, A. J.; Liu, X.; Kreidenweis, S. M.; Petters, M. D.; Twohy, C. H.; Richardson, M. S.; Eidhammer, T.; Rogers, D. C.; Tolbert, M. A. Predicting Global Atmospheric Ice Nuclei Distributions and Their Impacts on Climate. *PNAS* **2010**, *107* (25), 11217–11222. https://doi.org/doi.org/10.1073/pnas.0910818107.

(17) Kanji, Z. A. Chapter 1 Overview of Ice Nucleating Particles. *Meteor. Monogr.* **2017**, *58*, 1–33. https://doi.org/10.1175/AMSMONOGRAPHS-D-16-0006.1.

(18) Wallace, J. M.; Hobbs, P. V. Microphysics of Cold Clouds. In *Atmospheric Science: An Introductory Survey*; Elsevier Inc., 2006; pp 232–245.

(19) Chen, Y.; Demott, P. J.; Kreidenweis, S. M.; Rogers, D. C.; Sherman, D. E. Ice Formation by Sulfate and Sulfuric Acid Aerosol Particles under Upper-Tropospheric Conditions. *J Atmos Sci* **2000**, *57*, 3752–3766.

(20) Koop, T.; Luo, B.; Tsias, A.; Peter, T. Water Activity as the determinant for Homogeneous Ice nucleation in Aqueous Solutions. *Nature* **2000**, *406*, 611–614.

(21) DeMott, P. J.; Cziczo, D. J.; Prenni, A. J.; Murphy, D. M.; Kreidenweis, S. M.; Thomson, D. S.; Borys, R.; Rogers, D. C. Measurements of the Concentration and Composition of Nuclei for Cirrus Formation. *PNAS* **2003**, *100* (25), 14655–14660.

(22) Raatikainen, T.; Prank, M.; Ahola, J.; Kokkola, H.; Tonttila, J.; Romakkaniemi, S. The Effect of Marine Ice-Nucleating Particles on Mixed-Phase Clouds. *Atmos Chem Phys* **2022**, *22* (6), 3763–3778. https://doi.org/10.5194/acp-22-3763-2022.

(23) Fletcher, N. H. Active Sites and Ice Crystal Nucleation. *J Atmos Sci* **1969**, *26*, 1266–1271.

(24) DeMott, P. J.; Rogers, D. C.; Kreidenweis, S. M. The Susceptibility of Ice Formation in Upper Tropospheric Clouds to Insoluble Aerosol Components. *Journal of Geophysical Research Atmospheres* **1997**, *102* (16), 19575–19584. https://doi.org/10.1029/97jd01138.

(25) Ansmann, A.; Tesche, M.; Althausen, D.; Müller, D.; Seifert, P.; Freudenthaler, V.; Heese, B.; Wiegner, M.; Pisani, G.; Knippertz, P.; Dubovik, O. Influence of Saharan Dust on Cloud Glaciation in Southern Morocco during the Saharan Mineral Dust Experiment. *Journal of Geophysical Research Atmospheres* **2008**, *113* (4), 1–16. https://doi.org/10.1029/2007JD008785.

(26) Sear, R. P. Nucleation at Contact Lines Where Fluid-Fluid Interfaces Meet Solid Surfaces. *Journal of Physics Condensed Matter* **2007**, *19* (46), 1–8. https://doi.org/10.1088/0953-8984/19/46/466106.

(27) Cooper, W. A. A Possible Mechanism for Contact Nucleation. *J Atmos Sci* **1974**, *31*, 1832–1837.

(28) Ladino Moreno, L. A.; Stetzer, O.; Lohmann, U. Contact Freezing: A Review of Experimental Studies. *Atmos Chem Phys* **2013**, *13* (19), 9745–9769. https://doi.org/10.5194/acp-13-9745-2013.

(29) Niehaus, J.; Cantrell, W. Contact Freezing of Water by Salts. *Journal of Physical Chemistry Letters* **2015**, *6* (17), 3490–3495. https://doi.org/10.1021/acs.jpclett.5b01531.

(30) Durant, A. J.; Shaw, R. A. Evaporation Freezing by Contact Nucleation Inside-Out. *Geophys Res Lett* **2005**, *32* (20), 1–4. https://doi.org/10.1029/2005GL024175.

(31) Fornea, A. P.; Brooks, S. D.; Dooley, J. B.; Saha, A. Heterogeneous Freezing of Ice on Atmospheric Aerosols Containing Ash, Soot, and Soil. *Journal of Geophysical Research Atmospheres* **2009**, *114* (13), 1–12. https://doi.org/10.1029/2009JD011958.

(32) Brooks, S. D.; Suter, K.; Olivarez, L. Effects of Chemical Aging on the Ice Nucleation Activity of Soot and Polycyclic Aromatic Hydrocarbon Aerosols. *Journal of Physical Chemistry A* **2014**, *118* (43), 10036–10047. https://doi.org/10.1021/jp508809y.

(33) Collier, K. N.; Brooks, S. D. Role of Organic Hydrocarbons in Atmospheric Ice Formation via Contact Freezing. *Journal of Physical Chemistry A* **2016**, *120* (51), 10169–10180. https://doi.org/10.1021/acs.jpca.6b11890.

(34) Gurganus, C. W.; Charnawskas, J. C.; Kostinski, A. B.; Shaw, R. A. Nucleation at the Contact Line Observed on Nanotextured Surfaces. *Phys Rev Lett* **2014**, *113* (23), 1–5. https://doi.org/10.1103/PhysRevLett.113.235701.

(35) Marcolli, C.; Nagare, B.; Welti, A.; Lohmann, U. Ice Nucleation Efficiency of AgI: Review and New Insights. *Atmospheric Chemistry and Physics*. Copernicus GmbH July 19, 2016, pp 8915–8937. https://doi.org/10.5194/acp-16-8915-2016.

(36) Davis, R. D.; Tolbert, M. A. Crystal Nucleation Initiated by Transient Ion-Surface Interactions at Aerosol Interfaces. *Sci Adv* **2017**, *3* (7), 1–8. https://doi.org/10.1126/sciadv.1700425.

(37) Schiffman, Z. R.; Fernanders, M. S.; Davis, R. D.; Tolbert, M. A. Metal Oxide Particles as Atmospheric Nuclei: Exploring the Role of Metal Speciation in Heterogeneous Efflorescence and Ice Nucleation. *ACS Earth Space Chem* **2023**, *7* (4), 812–822. https://doi.org/10.1021/acsearthspacechem.2c00370.

(38) Young, K. C. The Role of Contact Nucleation in Ice Phase Initiation in Clouds. *J Atmos Sci* **1974**, *31* (3), 768–776.

(39) Seifert, P.; Ansmann, A.; Groß, S.; Freudenthaler, V.; Heinold, B.; Hiebsch, A.; Mattis, I.; Schmidt, J.; Schnell, F.; Tesche, M.; et al. Ice Formation in Ash-Influenced Clouds after the Eruption of the Eyjafjallajkull Volcano in April 2010. *Journal of Geophysical Research Atmospheres* **2011**, *116* (18), 1. https://doi.org/10.1029/2011JD015702.

(40) Ansmann, A.; Mattis, I.; Müller, D.; Wandinger, U.; Radlach, M.; Althausen, D.; Damoah, R. Ice Formation in Saharan Dust over Central Europe Observed with Temperature/Humidity/Aerosol Raman Lidar. *Journal of Geophysical Research D: Atmospheres* **2005**, *110* (18), 1–12. https://doi.org/10.1029/2004JD005000.

(41) Irish, V. E.; Hanna, S. J.; Willis, M. D.; China, S.; Thomas, J. L.; Wentzell, J. J. B.; Cirisan, A.; Si, M.; Leaitch, W. R.; Murphy, J. G.; et al. Ice Nucleating Particles in the Marine Boundary Layer in the Canadian Arctic during Summer 2014. *Atmos Chem Phys* **2019**, *19* (2), 1027–1039. https://doi.org/10.5194/acp-19-1027-2019.

(42) Isono, K.; Komabayasi, M.; Ono, A. The Nature and the Origin of Ice Nuclei in the Atmosphere. *Journ. Met. Soc. Japan* **1959**, *37*, 211–233.

(43) Kumai, M. Snow Crystals and the Identification of the Nuclei in the Northern United States of America. *Journal of Meteorology* **1961**, 139–150.

(44) Zuberi, B.; Bertram, A. K.; Cassa, C. A.; Molina, L. T.; Molina, M. J. Heterogeneous Nucleation of Ice in (NH4)2SO4-H2O Particles with Mineral Dust Immersions. *Geophys Res Lett* **2002**, *29* (10), 142.1-142.4. https://doi.org/10.1029/2001gl014289.

(45) Sassen, K. Indirect Climate Forcing over the Western US from Asian Dust Storms. *Geophys Res Lett* **2002**, *29* (10), 103-1-103–104. https://doi.org/10.1029/2001gl014051.

(46) DeMott, P. J.; Sassen, K.; Poellot, M. R.; Baumgardner, D.; Rogers, D. C.; Brooks, S. D.; Prenni, A. J.; Kreidenweis, S. M. African Dust Aerosols as Atmospheric Ice Nuclei. *Geophys Res Lett* **2003**, *30* (14), 1.1-1.4. https://doi.org/10.1029/2003GL017410.

(47) Sassen, K. Dusty Ice Clouds over Alaska. *Nature* **2005**, *434*, 456.

(48) Archuleta, C. M.; DeMott, P. J.; Kreidenweis, S. M. Ice Nucleation by Surrogates for Atmospheric Mineral Dust and Mineral Dust/Sulfate Particles at Cirrus Temperatures. *Atmos Chem Phys* **2005**, *5* (10), 2617–2634. https://doi.org/10.5194/acp-5-2617-2005.

(49) Marcolli, C.; Gedamke, S.; Peter, T.; Zobrist, B. Efficiency of Immersion Mode Ice Nucleation on Surrogates of Mineral Dust. *Atmos. Chem. Phys* **2007**, *7*, 5081–5091.

(50) Broadley, S. L.; Murray, B. J.; Herbert, R. J.; Atkinson, J. D.; Dobbie, S.; Malkin, T. L.; Condliffe, E.; Neve, L. Immersion Mode Heterogeneous Ice Nucleation by an Illite Rich Powder Representative of Atmospheric Mineral Dust. *Atmos Chem Phys* **2012**, *12* (1), 287–307. https://doi.org/10.5194/acp-12-287-2012.

(51) Yakobi-Hancock, J. D.; Ladino, L. A.; Abbatt, J. P. D. Feldspar Minerals as Efficient Deposition Ice Nuclei. *Atmos Chem Phys* **2013**, *13* (22), 11175–11185. https://doi.org/10.5194/acp-13-11175-2013.

(52) Atkinson, J. D.; Murray, B. J.; Woodhouse, M. T.; Whale, T. F.; Baustian, K. J.; Carslaw, K. S.; Dobbie, S.; O'Sullivan, D.; Malkin, T. L. The Importance of Feldspar for Ice Nucleation by Mineral Dust in Mixed-Phase Clouds. *Nature* **2013**, *498* (7454), 355–358. https://doi.org/10.1038/nature12278.

(53) Harrison, A. D.; Whale, T. F.; Carpenter, M. A.; Holden, M. A.; Neve, L.; Sullivan, D. O.; Temprado, J. V.; Murray, B. J. Not All Feldspars Are Equal : A Survey of Ice Nucleating Properties across the Feldspar Group of Minerals. *Atmos. Chem. Phys.* **2016**, *16*, 10927–10940. https://doi.org/10.5194/acp-16-10927-2016.

(54) Harrison, A. D.; Lever, K.; Sanchez-Marroquin, A.; Holden, M. A.; Whale, T. F.; Tarn, M. D.; McQuaid, J. B.; Murray, B. J. The Ice-Nucleating Ability of Quartz Immersed in Water and Its Atmospheric Importance Compared to K-Feldspar. *Atmos Chem Phys* **2019**, *19* (17), 11343–11361. https://doi.org/10.5194/acp-19-11343-2019.

(55) DeMott, P. J.; Chen, Y.; Kreidenweis, S. M.; Rogers, D. C.; Sherman, D. E. Ice Formation by Black Carbon Particles. *Geophys Res Lett* **1999**, *26* (16), 2429–2432. https://doi.org/10.1029/1999GL900580.

(56) Friedman, B.; Kulkarni, G.; Beránek, J.; Zelenyuk, A.; Thornton, J. A.; Cziczo, D. J. Ice Nucleation and Droplet Formation by Bare and Coated Soot Particles. *Journal of Geophysical Research Atmospheres* **2011**, *116* (17), 1–11. https://doi.org/10.1029/2011JD015999.

(57) Jensen, E. J.; Toon, O. B. The Potential Effects of Volcanic Aerosols on Cirrus Cloud Microphysics. *Geophys Res Lett* **1992**, *19* (17), 1759–1762. https://doi.org/10.1029/92GL01936.

(58) Jahn, L. G.; Fahy, W. D.; Williams, D. B.; Sullivan, R. C. Role of Feldspar and Pyroxene Minerals in the Ice Nucleating Ability of Three Volcanic Ashes. *ACS Earth Space Chem* **2019**, *3* (4), 626–636. https://doi.org/10.1021/acsearthspacechem.9b00004.

(59) Schwidetzky, R.; de Almeida Ribeiro, I.; Bothen, N.; Backes, A. T.; DeVries, A. L.; Bonn, M.; Fröhlich-Nowoisky, J.; Molinero, V.; Meister, K. Functional Aggregation of Cell-Free Proteins Enables Fungal Ice Nucleation. *Proc Natl Acad Sci U S A* **2023**, *120* (46), 1–7. https://doi.org/10.1073/pnas.2303243120.

(60) Thornton, D. C. O.; Brooks, S. D.; Wilbourn, E. K.; Mirrielees, J.; Alsante, A. N.; Gold-Bouchot, G.; Whitesell, A.; McFadden, K. Production of Ice-Nucleating Particles (INPs) by Fast-Growing Phytoplankton. *Atmos Chem Phys* **2023**, *23* (19), 12707–12729. https://doi.org/10.5194/acp-23-12707-2023.

(61) Matthews, B. H.; Alsante, A. N.; Brooks, S. D. Pollen Emissions of Subpollen Particles and Ice Nucleating Particles. *ACS Earth Space Chem* **2023**, *7* (6), 1207–1218. https://doi.org/10.1021/acsearthspacechem.3c00014.

(62) Alsante, A. N.; Thornton, D. C. O.; Brooks, S. D. Effect of Aggregation and Molecular Size on the Ice Nucleation Efficiency of Proteins. *Environ Sci Technol* **2024**, *58* (10), 4594–4605. https://doi.org/10.1021/acs.est.3c06835.

(63) Bieber, P.; Borduas-Dedekind, N. High-Speed Cryo-Microscopy Reveals That Ice-Nucleating Proteins of Pseudomonas Syringae Trigger Freezing at Hydrophobic Interfaces. *Sci. Adv* **2024**, *10* (27), 1–11. https://doi.org/DOI:10.1126/sciadv.adn6606.

(64) Alden, K. A.; Bieber, P.; Miller, A. J.; Link, N.; Murray, B. J.; Borduas-Dedekind, N. The Role of Surface-Active Macromolecules in the Ice-Nucleating Ability of Lignin, Snomax, and Agricultural Soil Extracts. *Atmos Chem Phys* **2025**, *25* (12), 6179–6195. https://doi.org/10.5194/acp-25-6179-2025.

(65) Komabayasi, M.; Ikebe, Y. Organic Ice Nuclei : Ice-Forming Properties of Some Aromatic Compounds. *Journ. Met. Soc. Japan* **1961**, *39*, 82–94.

(66) Fukuta, N. Experimental Studies of Organic Ice Nuclei. *J Atmos Sci* **1966**, *23*, 191–196.

(67) Edwards, G. R.; Evans, L. F. The Mechanism of Activation of Ice Nuclei. *J Atmos Sci* **1971**, *28*, 1443–1447.

(68) Knopf, D. A.; Alpert, P. A.; Wang, B. The Role of Organic Aerosol in Atmospheric Ice Nucleation: A Review. *ACS Earth Space Chem* **2018**, *2*, 168–202. https://doi.org/10.1021/acsearthspacechem.7b00120.

(69) Cziczo, D. J.; Froyd, K. D.; Hoose, C.; Jensen, E. J.; Diao, M.; Zondlo, M. A.; Smith, J. B.; Twohy, C. H.; Murphy, D. M. Clarifying the Dominant Sources and Mechanisms of Cirrus Cloud Formation. *Science (1979)* **2013**, *340* (June), 1320–1325.

(70) Knopf, D. A.; Wang, P.; Wong, B.; Tomlin, J. M.; Veghte, D. P.; Lata, N. N.; China, S.; Laskin, A.; Moffet, R. C.; Aller, J. Y.; et al. Physicochemical Characterization of Free Troposphere and Marine Boundary Layer Ice-Nucleating Particles Collected by Aircraft in the Eastern North Atlantic. *Atmos Chem Phys* **2023**, *23* (15), 8659–8681. https://doi.org/10.5194/acp-23-8659-2023.

(71) Knopf, D. A.; Charnawskas, J. C.; Wang, P.; Wong, B.; Tomlin, J. M.; Jankowski, K. A.; Fraund, M.; Veghte, D. P.; China, S.; Laskin, A.; et al. Micro-Spectroscopic and Freezing Characterization of Ice-Nucleating Particles Collected in the Marine Boundary Layer in the Eastern North Atlantic. *Atmos Chem Phys* **2022**, *22* (8), 5377–5398. https://doi.org/10.5194/acp-22-5377-2022.

(72) Fletcher, A. N. High-Temperature Contact Nucleation of Supercooled Water by Organic Chemicals. *Journal of Applied Meteorology* **1972**, *11*, 988–993.

(73) DeMott, P. J.; Mason, R. H.; McCluskey, C. S.; Hill, T. C. J.; Perkins, R. J.; Desyaterik, Y.; Bertram, A. K.; Trueblood, J. V.; Grassian, V. H.; Qiu, Y.; et al. Ice Nucleation by Particles Containing Long-Chain Fatty Acids of Relevance to Freezing by Sea Spray Aerosols. *Environ Sci Process Impacts* **2018**, *20* (11), 1559–1569. https://doi.org/10.1039/c8em00386f.

(74) Wise, M. E.; Baustian, K. J.; Tolbert, M. A. Internally Mixed Sulfate and Organic Particles as Potential Ice Nuclei in the Tropical Tropopause Region. *Proc Natl Acad Sci U S A* **2010**, *107* (15), 6693–6698. https://doi.org/10.1073/pnas.0913018107.

(75) Baustian, K. J.; Wise, M. E.; Tolbert, M. A. Depositional Ice Nucleation on Solid Ammonium Sulfate and Glutaric Acid Particles. *Atmos. Chem. Phys* **2010**, *10*, 2307–2317.

(76) Schill, G. P.; Tolbert, M. A. Heterogeneous Ice Nucleation on Phase-Separated Organic-Sulfate Particles: Effect of Liquid vs. Glassy Coatings. *Atmos Chem Phys* **2013**, *13* (9), 4681–4695. https://doi.org/10.5194/acp-13-4681-2013.

(77) Schill, G. P.; De Haan, D. O.; Tolbert, M. A. Heterogeneous Ice Nucleation on Simulated Secondary Organic Aerosol. *Environ Sci Technol* **2014**, *48* (3), 1675–1682. https://doi.org/10.1021/es4046428.

(78) Baustian, K. J.; Wise, M. E.; Jensen, E. J.; Schill, G. P.; Freedman, M. A.; Tolbert, M. A. State Transformations and Ice Nucleation in Amorphous (Semi-)Solid Organic Aerosol. *Atmos Chem Phys* **2013**, *13* (11), 5615–5628. https://doi.org/10.5194/acp-13-5615-2013.

(79) Buck, A. L. New Equations for Computing Vapor Pressure and Enhancement Factor. *Journal of Applied Meteorology* **1981**, *20*, 1527–1532.

(80) Marti, J.; Mauersberger, K. A Survey and New Measurements of Ice Vapor Pressure at Temperatures between 170 and 250K. *Geophys Res Lett* **1993**, *20* (5), 363–366. https://doi.org/10.1029/93GL00105.

(81) Martin, S. T. Phase Transitions of Aqueous Atmospheric Particles. *Chem Rev* **2000**, *100* (9), 3403–3453. https://doi.org/10.1021/cr990034t.

(82) Hung, H. M.; Malinowski, A.; Martin, S. T. Ice Nucleation Kinetics of Aerosols Containing Aqueous and Solid Ammonium Sulfate Particles. *Journal of Physical Chemistry A* **2002**, *106* (2), 293–306. https://doi.org/10.1021/jp012064h.

(83) Duričković, I.; Claverie, R.; Bourson, P.; Marchetti, M.; Chassot, J. M.; Fontana, M. D. Water-Ice Phase Transition Probed by Raman Spectroscopy. *Journal of Raman Spectroscopy* **2011**, *42* (6), 1408–1412. https://doi.org/10.1002/jrs.2841.

(84) Yalkowsky, S. H.; He, Y.; Jain, P. *Handbook of Aqueous Solubility Data*, 2nd ed.; CRC Press: Boca Raton, FL, 2010.

(85) Bretti, C.; Crea, F.; Foti, C.; Sammartano, S. Solubility and Activity Coefficients of Acidic and Basic Nonelectrolytes in Aqueous Salt Solutions. 2. Solubility and Activity Coefficients of Suberic, Azelaic, and Sebacic Acids in NaCl(Aq), (CH3)4NCl(Aq), and (C2H5)4NI(Aq) at Different Ionic Strengths and at t = 25 °C. *J Chem Eng Data* **2006**, *51* (5), 1660–1667. https://doi.org/10.1021/je060132t.

(86) Park, C.; Sheehan, R. J. Phthalic Acids and Other Benzenepolycarboxylic Acids. In *Kirk-Othmer Encyclopedia of Chemical Technology*; John Wiley & Sons, Inc., 2000. https://doi.org/10.1002/0471238961.1608200816011811.a01.

(87) Zhang, Y.; Guo, F.; Cui, Q.; Lu, M.; Song, X.; Tang, H.; Li, Q. Measurement and Correlation of the Solubility of Vanillic Acid in Eight Pure and Water + Ethanol Mixed Solvents at Temperatures from (293.15 to 323.15) K. *J Chem Eng Data* **2016**, *61* (1), 420–429. https://doi.org/10.1021/acs.jced.5b00619.

(88) Tellez, C. A.; Hollauer, E.; Mondragon, M. A.; Castano, V. M. Fourier Transform Infrared and Raman Spectra, Vibrational Assignment and Ab Initio Calculations of Terephthalic Acid and Related Compounds. *Spectrochim Acta A Mol Biomol Spectrosc* **2001**, *57* (5), 993–1007.

(89) Xu, L.; Fang, Y. Raman Spectroscopy of P-Hydroxybenzoic Acid Aqueous Solution and Surface-Unenhanced Raman Scattering on Silver Colloid with Ultraviolet Excitation. *J Colloid Interface Sci* **2004**, *274* (1), 122–125. https://doi.org/10.1016/j.jcis.2003.12.041.

(90) Benítez, A.; Amaro-Gahete, J.; Esquivel, D.; Romero-Salguero, F. J.; Morales, J.; Caballero, Á. MIL-88A Metal-Organic Framework as a Stable Sulfur-Host Cathode for Long-Cycle Li-S Batteries. *Nanomaterials* **2020**, *10* (424), 1–14. https://doi.org/10.3390/nano10030424.

(91) Tourwé, E.; Baert, K.; Hubin, A. Surface-Enhanced Raman Scattering (SERS) of Phthalic Acid and 4-Methyl Phthalic Acid on Silver Colloids as a Function of PH. *Vib Spectrosc* **2006**, *40* (1), 25–32. https://doi.org/10.1016/j.vibspec.2005.06.005.

(92) *PINONIC ACID(61826-55-9) Raman*. Chemical Book. https://www.chemicalbook.com/SpectrumEN_61826-55-9_Raman.htm (accessed 2024-11-18).

(93) Carrizo, D.; Muñoz-Iglesias, V.; Fernández-Sampedro, M. T.; Gil-Lozano, C.; Sánchez-García, L.; Prieto-Ballesteros, O.; Medina, J.; Rull, F. Detection of Potential Lipid Biomarkers in Oxidative Environments by Raman Spectroscopy and Implications for the Exomars 2020-Raman Laser Spectrometer Instrument Performance. *Astrobiology* **2020**, *20* (3), 405–414. https://doi.org/10.1089/ast.2019.2100.

(94) *Sebacic acid(111-20-6) Raman*. Chemical Book. https://www.chemicalbook.com/SpectrumEN_111-20-6_Raman.htm (accessed 2024-12-18).

(95) Martini, W. S.; Porto, B. L. S.; De Oliveira, M. A. L.; Sant'Ana, A. C. Comparative Study of the Lipid Profiles of Oils from Kernels of Peanut, Babassu, Coconut, Castor and Grape by GC-FID and Raman Spectroscopy. *J Braz Chem Soc* **2018**, *29* (2), 390–397. https://doi.org/10.21577/0103-5053.20170152.

(96) Suzuki, M.; Shimanouchi, T. Infrared and Raman Spectra of Adipic Acid Crystal. *J Mol Spectrosc* **1969**, *29*, 415–425.

(97) Clavijo, E.; Menéndez, J. R.; Aroca, R. Vibrational and Surface-Enhanced Raman Spectra of Vanillic Acid. *Journal of Raman Spectroscopy* **2008**, *39* (9), 1178–1182. https://doi.org/10.1002/jrs.1959.

(98) Ryland, A. L. X-Ray Diffraction. *J Chem Educ* **1958**, *35* (2), 80–83.

(99) Vali, G. Repeatability and Randomness in Heterogeneous Freezing Nucleation. *Atmos. Chem. Phys* **2008**, *8*, 5017–5031. https://doi.org/doi.org/10.5194/acp-8-5017-2008.

(100) Bogler, S.; Borduas-Dedekind, N. Lignin's Ability to Nucleate Ice via Immersion Freezing and Its Stability towards Physicochemical Treatments and Atmospheric Processing. *Atmos Chem Phys* **2020**, *20* (23), 14509–14522. https://doi.org/10.5194/acp-20-14509-2020.

(101) Demott, P. J. Quantitative Descriptions of Ice Formation Mechanisms of Silver Iodide-Type Aerosols. *Atmos Res* **1995**, *38*, 63–99.

(102) Harris, D. C.; Lucy, C. A. Comparison of Means with Student's t. In *Quantitative Chemical Analysis*; MacMillan Learning: New York, NY, 2020; pp 77–81.

(103) Turnbull, D.; Vonnegut, B. Nucleation Catalysis. *Ind Eng Chem* **1952**, *44* (6), 1292–1298.

(104) Vonnegut, B. The Nucleation of Ice Formation by Silver Iodide. *J Appl Phys* **1947**, *18* (7), 593–595. https://doi.org/10.1063/1.1697813.

(105) Davis, R. D.; Lance, S.; Gordon, J. A.; Ushijima, S. B.; Tolbert, M. A. Contact Efflorescence as a Pathway for Crystallization of Atmospherically Relevant Particles. *Proc Natl Acad Sci U S A* **2015**, *112* (52), 15815–15820. https://doi.org/10.1073/pnas.1522860113.

(106) Ushijima, S. B.; Davis, R. D.; Tolbert, M. A. Immersion and Contact Efflorescence Induced by Mineral Dust Particles. *Journal of Physical Chemistry A* **2018**, *122* (5), 1303–1311. https://doi.org/10.1021/acs.jpca.7b12075.

(107) McMillan, K. A.; Davis, R. D.; Tolbert, M. A. Crystalline Organic Compounds as Effective Nuclei in Contact Efflorescence of Ammonium Sulfate. *Journal of Physical Chemistry A* **2025**, *129* (9), 2296–2307. https://doi.org/10.1021/acs.jpca.4c07566.

(108) Fitzner, M.; Sosso, G. C.; Cox, S. J.; Michaelides, A. The Many Faces of Heterogeneous Ice Nucleation: Interplay between Surface Morphology and Hydrophobicity. *J Am Chem Soc* **2015**, *137* (42), 13658–13669. https://doi.org/10.1021/jacs.5b08748.

(109) Fitzner, M.; Pedevilla, P.; Michaelides, A. Predicting Heterogeneous Ice Nucleation with a Data-Driven Approach. *Nat Commun* **2020**, *11* (4777), 1–9. https://doi.org/10.1038/s41467-020-18605-3.

(110) Davis, R. D.; Lance, S.; Gordon, J. A.; Tolbert, M. A. Long Working-Distance Optical Trap for in Situ Analysis of Contact-Induced Phase Transformations. *Anal Chem* **2015**, *87* (12), 6186–6194. https://doi.org/10.1021/acs.analchem.5b00809.

(111) Anbu Chudar Azhagan, S.; Marianandhakumar, V. Crystallization of Pure Adipic Acid from Methanol Solvent and Their Characterization Studies: Intense NLO Activity from Centrosymmetric Crystal. *Optik (Stuttg)* **2021**, *227*, 1–5. https://doi.org/10.1016/j.ijleo.2020.166002.

(112) Lalancette, R. A.; Thompson, H. W.; Brunskill, A. P. J. (+)-Cis-Pinonic Acid: Catemeric Hydrogen Bonding in a Non-Racemic e-Keto Acid. *Acta Cryst.* **1999**, *C55*, 1908–1911.

(113) Bednowitz, A. L.; Post, B. Direct Determination of the Crystal Structure of Beta-Fumaric Acid. *Acta Cryst* **1966**, *21*, 566–571.

(114) Heath, E. A.; Singh, P.; Ebisuzaki, Y. Structure of P-Hydroxybenzoic Acid and p-Hydroxybenzoic Acid-Acetone (2/1). *Acta Cryst* **1992**, *C48*, 1960–1965.

(115) Frede, E.; Precht, D. Crystal Structures of Binary Systems of Saturated Fatty Acids. *J Am Oil Chem Soc* **1976**, *53*, 668–670.

(116) Suresh Kumar, M.; Rajesh, K.; Vijayaraghavan, G. V.; Krishnan, S. Growth, Structural and Mechanical Studies of Phthalic Acid Single Crystals Grown in Two Different Solutions. *Mater Res Express* **2018**, *5* (11), 1–8. https://doi.org/10.1088/2053-1591/aadd81.

(117) Von Sydow, E. On the Structure of the Crystal Form B of Stearic Acid. *Acta Cryst.* **1955**, *8*, 557–560.

(118) Röttger, K.; Endriss, A.; Ihringer, J.; Doyle, S.; Kuhs, W. F. Erratum: Lattice Constants and Thermal Expansion of H 2O and D 2O Ice Ih between 10 and 265 K (Acta Crystallographica Section B: Structural Science (1994) B50 (644-648)). *Acta Crystallographica Section B: Structural Science*. February 2012, p 91. https://doi.org/10.1107/S0108768111046908.

(119) Ray, S.; Savoie, B. M.; Dudareva, N.; Morgan, J. A. Diffusion of Volatile Organics and Water in the Epicuticular Waxes of Petunia Petal Epidermal Cells. *Plant Journal* **2022**, *110* (3), 658–672. https://doi.org/10.1111/tpj.15693.

(120) Thalladi, V. R.; Nüsse, M.; Boese, R. The Melting Point Alternation in α,ω-Alkanedicarboxylic Acids. *J Am Chem Soc* **2000**, *122* (38), 9227–9236. https://doi.org/10.1021/ja0011459.

(121) Fischer, P.; Zolliker, P.; Meier, B. H.; Ernst, R. R.; Hewat, A. W.; Jorgensen, J. D.; Rotella, F. J. Structure and Dynamics of Terephthalic Acid from 2 to 300 K 1. High-Resolution Neutron Diffraction Evidence for a Temperature-Dependent Order-Disorder Transition: A Comparison of Reactor and Pulsed Neutron Source Powder Techniques. *J Solid State Chem* **1986**, *61* (1), 109–125.

(122) Kozlevčar, B.; Odlazek, D.; Golobič, A.; Pevec, A.; Strauch, P.; Šegedin, P. Complexes with Lignin Model Compound Vanillic Acid. Two Different Carboxylate Ligands in the Same Dinuclear Tetracarboxylate Complex [Cu 2(C8H7O4)2(O 2CCH3)2(CH3OH)2]. *Polyhedron* **2006**, *25* (5), 1161–1166. https://doi.org/10.1016/j.poly.2005.08.031.

(123) Cava, R. J.; Reidinger, F.; Wuensch, B. J. SINGLE-CRYSTAL NEUTRON-DIFFRACTION STUDY OF AgI BETWEEN 23° AND 300°C. *Solid State Commun* **1977**, *24*, 411–416.

(124) Gavish, M.; Popovitz-Biro, R.; Lahav, M.; Leiserowitz, L. Ice Nucleation by Alcohols Arranged in Monolayers at the Surface of Water Drops. *Science (1979)* **1990**, *250*, 973–975.

(125) Popovitz-Biro, R.; Wang, J. L.; Majewski, J.; Sbavit, E.; Leiserowitz, L.; Lahav, M. Induced Freezing of Supercooled Water into Ice by Self-Assembled Crystalline Monolayers of Amphiphilic Alcohols at the Air-Water Interface. *J. Am. Chem. Soc* **1994**, *116*, 1179–1191.

(126) Majewski, J.; Popovitz-Biro, R.; Bouwman, W. G.; Kjaer, K.; Als-Nielsen, J.; Lahav, M.; Leiserowitz, L. The Structural Properties of Uncompressed Crystalline Monolayers of

Alcohols CnH2n+1 OH (n = 13–31) on Water and Their Role as Ice Nucleators. *Chemistry – A European Journal* **1995**, *1* (5), 304–311. https://doi.org/10.1002/chem.19950010507.

(127) Ochshorn, E.; Cantrell, W. Towards Understanding Ice Nucleation by Long Chain Alcohols. *Journal of Chemical Physics* **2006**, *124* (5), 054714.1-054714.6. https://doi.org/10.1063/1.2166368.

(128) Qiu, Y.; Odendahl, N.; Hudait, A.; Mason, R.; Bertram, A. K.; Paesani, F.; DeMott, P. J.; Molinero, V. Ice Nucleation Efficiency of Hydroxylated Organic Surfaces Is Controlled by Their Structural Fluctuations and Mismatch to Ice. *J Am Chem Soc* **2017**, *139* (8), 3052–3064. https://doi.org/10.1021/jacs.6b12210.

(129) Pharoah, L.; Bertram, A. K.; Patey, G. N. The Mechanism of Heterogeneous Ice Nucleation by Fatty Alcohol Monolayers. *Journal of Physical Chemistry A* **2024**, *128* (34), 7214–7225. https://doi.org/10.1021/acs.jpca.4c03912.

(130) Zielke, S. A.; Bertram, A. K.; Patey, G. N. Simulations of Ice Nucleation by Kaolinite (001) with Rigid and Flexible Surfaces. *Journal of Physical Chemistry B* **2016**, *120* (8), 1726–1734. https://doi.org/10.1021/acs.jpcb.5b09052.

(131) Fukuta, N.; Mason, B. J. EPITAXIAL GROWTH OF ICE ON ORGANIC CRYSTALS. *J. Phys. Chem. Solids* **1963**, *24*, 715–718.

(132) Lupi, L.; Molinero, V. Does Hydrophilicity of Carbon Particles Improve Their Ice Nucleation Ability? *Journal of Physical Chemistry A* **2014**, *118* (35), 7330–7337. https://doi.org/10.1021/jp4118375.

(133) Cox, S. J.; Kathmann, S. M.; Slater, B.; Michaelides, A. Molecular Simulations of Heterogeneous Ice Nucleation. I. Controlling Ice Nucleation through Surface Hydrophilicity. *Journal of Chemical Physics* **2015**, *142* (18), 184704.1-184704.5. https://doi.org/10.1063/1.4919714.

(134) Cox, S. J.; Kathmann, S. M.; Slater, B.; Michaelides, A. Molecular Simulations of Heterogeneous Ice Nucleation. II. Peeling Back the Layers. *Journal of Chemical Physics* **2015**, *142* (18), 184705.1-184705.8. https://doi.org/10.1063/1.4919715.

(135) Prenni, A. J.; DeMott, P. J.; Kreidenweis, S. M.; Sherman, D. E.; Russell, L. M.; Ming, Y. The Effects of Low Molecular Weight Dicarboxylic Acids on Cloud Formation. *Journal of Physical Chemistry A* **2001**, *105* (50), 11240–11248. https://doi.org/10.1021/jp012427d.

(136) Mehndiratta, L.; Lyp, A. E.; Slade, J. H.; Grassian, V. H. Immersion Ice Nucleation of Atmospherically Relevant Lipid Particles. *Environmental Science: Atmospheres* **2024**, *4* (11), 1239–1254. https://doi.org/10.1039/d4ea00066h.

(137) Silberberg, M. S.; Amateis, P. The Properties of Mixtures: Solutions and Colloids. In *Chemistry: The Molecular Nature of Matter and Change*; McGraw-Hill Education: New York, NY, 2015; pp 516–567.

(138) Nichman, L.; Wolf, M.; Davidovits, P.; Onasch, T. B.; Zhang, Y.; Worsnop, D. R.; Bhandari, J.; Mazzoleni, C.; Cziczo, D. J. Laboratory Study of the Heterogeneous Ice Nucleation on Black-Carbon-Containing Aerosol. *Atmos Chem Phys* **2019**, *19* (19), 12175–12194. https://doi.org/10.5194/acp-19-12175-2019.

(139) Zobrist, B.; Marcolli, C.; Koop, T.; Luo, B. P.; Murphy, D. M.; Lohmann, U.; Zardini, A. A.; Krieger, U. K.; Corti, T.; Cziczo, D. J.; et al. Oxalic Acid as a Heterogeneous Ice Nucleus in the Upper Troposphere and Its Indirect Aerosol Effect. *Atmos. Chem. Phys* **2006**, *6*, 3115–3129.

(140) Zobrist, B.; Koop, T.; Luo, B. P.; Marcolli, C.; Peter, T. Heterogeneous Ice Nucleation Rate Coefficient of Water Droplets Coated by a Nonadecanol Monolayer. *Journal of Physical Chemistry C* **2007**, *111* (5), 2149–2155. https://doi.org/10.1021/jp066080w.

(141) Perkins, R. J.; Vazquez De Vasquez, M. G.; Beasley, E. E.; Hill, T. C. J.; Stone, E. A.; Allen, H. C.; Demott, P. J. Relating Structure and Ice Nucleation of Mixed Surfactant Systems Relevant to Sea Spray Aerosol. *Journal of Physical Chemistry A* **2020**, *124* (42), 8806–8821. https://doi.org/10.1021/acs.jpca.0c05849.

(142) Murphy, D. M.; Cziczo, D. J.; Froyd, K. D.; Hudson, P. K.; Matthew, B. M.; Middlebrook, A. M.; Peltier, R. E.; Sullivan, A.; Thomson, D. S.; Weber, R. J. Single-Particle Mass Spectrometry of Tropospheric Aerosol Particles. *Journal of Geophysical Research Atmospheres* **2006**, *111* (23), 1–15. https://doi.org/10.1029/2006JD007340.

(143) Zhang, Q.; Jimenez, J. L.; Canagaratna, M. R.; Allan, J. D.; Coe, H.; Ulbrich, I.; Alfarra, M. R.; Takami, A.; Middlebrook, A. M.; Sun, Y. L.; et al. Ubiquity and Dominance of Oxygenated Species in Organic Aerosols in Anthropogenically-Influenced Northern Hemisphere Midlatitudes. *Geophys Res Lett* **2007**, *34* (13), 1–6. https://doi.org/10.1029/2007GL029979.

(144) Ehn, M.; Thornton, J. A.; Kleist, E.; Sipilä, M.; Junninen, H.; Pullinen, I.; Springer, M.; Rubach, F.; Tillmann, R.; Lee, B.; et al. A Large Source of Low-Volatility Secondary Organic Aerosol. *Nature* **2014**, *506* (7489), 476–479. https://doi.org/10.1038/nature13032.

(145) Jimenez, J. L.; Canagaratna, M. R.; Donahue, N. M.; Prevot, A. S. H.; Zhang, Q.; Kroll, J. H.; DeCarlo, P. F.; Allan, J. D.; Coe, H.; Ng, N. L.; Aiken, A. C.; Docherty, K. S.; Ulbrich, I. M.; Grieshop, A. P.; Robinson, A. L.; Duplissy, J.; Smith, J. D.; Wilson, K. R.; Lanz, V. A.; Hueglin, C.; Sun, Y. L.; Tian, J.; Laaksonen, A.; Raatikainen, T.; Rautiainen, J.; Vaattovaara, P.; Ehn, M.; Kulmala, M.; Tomlinson, J. M.; Collins, D. R.; Cubison, M. J.; Dunlea, E. J.; Huffman, J. A.; Onasch, T. B.; Alfarra, M. R.; Williams, P. I.; Bower, K.; Kondo, Y.; Schneider, J.; Drewnick, F.; Borrmann, S.; Weimer, S.; Demerjian, K.; Salcedo, D.; Cottrell, L.; Griffin, R.; Takami, A.; Miyoshi, T.; Hatakeyama, S.; Shimono, A.; Sun, J. Y.; Zhang, Y. M.; Dzepina, K.; Kimmel, J. R.; Sueper, D.; Jayne, J. T.; Herndon, S. C.; Trimborn, A. M.; Williams, L. R.; Wood, E. C.; Middlebrook, A. M.; Kolb, C. E.; Baltensperger, U.; Worsnop, D. R. Evolution of Organic Aerosols in the

Atmosphere. *Science (1979)* **2009**, *326* (5959), 1525–1529. https://doi.org/10.1126/science.1180353.

(146) Wilson, T. W.; Murray, B. J.; Wagner, R.; Möhler, O.; Saathoff, H.; Schnaiter, M.; Skrotzki, J.; Price, H. C.; Malkin, T. L.; Dobbie, S.; et al. Glassy Aerosols with a Range of Compositions Nucleate Ice Heterogeneously at Cirrus Temperatures. *Atmos Chem Phys* **2012**, *12* (18), 8611–8632. https://doi.org/10.5194/acp-12-8611-2012.

(147) Wang, B.; Lambe, A. T.; Massoli, P.; Onasch, T. B.; Davidovits, P.; Worsnop, D. R.; Knopf, D. A. The Deposition Ice Nucleation and Immersion Freezing Potential of Amorphous Secondary Organic Aerosol: Pathways for Ice and Mixed-Phase Cloud Formation. *Journal of Geophysical Research Atmospheres* **2012**, *117* (16), 1–12. https://doi.org/10.1029/2012JD018063.

(148) Berkemeier, T.; Shiraiwa, M.; Pöschl, U.; Koop, T. Competition between Water Uptake and Ice Nucleation by Glassy Organic Aerosol Particles. *Atmos Chem Phys* **2014**, *14* (22), 12513–12531. https://doi.org/10.5194/acp-14-12513-2014.

(149) Murray, B. J.; Wilson, T. W.; Dobbie, S.; Cui, Z.; Al-Jumur, S. M. R. K.; Möhler, O.; Schnaiter, M.; Wagner, R.; Benz, S.; Niemand, M.; et al. Heterogeneous Nucleation of Ice Particles on Glassy Aerosols under Cirrus Conditions. *Nat Geosci* **2010**, *3* (4), 233–237. https://doi.org/10.1038/ngeo817.

(150) Wagner, R.; Möhler, O.; Saathoff, H.; Schnaiter, M.; Skrotzki, J.; Leisner, T.; Wilson, T. W.; Malkin, T. L.; Murray, B. J. Ice Cloud Processing of Ultra-Viscous/Glassy Aerosol Particles Leads to Enhanced Ice Nucleation Ability. *Atmos Chem Phys* **2012**, *12* (18), 8589–8610. https://doi.org/10.5194/acp-12-8589-2012.

(151) Ignatius, K.; Kristensen, T. B.; Järvinen, E.; Nichman, L.; Fuchs, C.; Gordon, H.; Herenz, P.; Hoyle, C. R.; Duplissy, J.; Garimella, S.; et al. Heterogeneous Ice Nucleation of Viscous Secondary Organic Aerosol Produced from Ozonolysis of α-Pinene. *Atmos Chem Phys* **2016**, *16* (10), 6495–6509. https://doi.org/10.5194/acp-16-6495-2016.

(152) Wagner, R.; Höhler, K.; Huang, W.; Kiselev, A.; Möhler, O.; Mohr, C.; Pajunoja, A.; Saathoff, H.; Schiebel, T.; Shen, X.; et al. Heterogeneous Ice Nucleation of α-Pinene SOA Particles before and after Ice Cloud Processing. *J Geophys Res* **2017**, *122* (9), 4924–4943. https://doi.org/10.1002/2016JD026401.

(153) Lohmann, U. Possible Aerosol Effects on Ice Clouds via Contact Nucleation. *J Atmos Sci* **2002**, *59*, 647–656.

(154) Marcolli, C. Deposition Nucleation Viewed as Homogeneous or Immersion Freezing in Pores and Cavities. *Atmos Chem Phys* **2014**, *14* (4), 2071–2104. https://doi.org/10.5194/acp-14-2071-2014.

(155) Diehl, K.; Matthias-Maser, S.; Jaenicke, R.; Mitra, S. K. The Ice Nucleating Ability of Pollen: Part II. Laboratory Studies in Immersion and Contact Freezing Modes. *Atmos Res* **2002**, *61*, 125–133.

(156) Shaw, R. A.; Durant, A. J.; Mi, Y. Heterogeneous Surface Crystallization Observed in Undercooled Water. *Journal of Physical Chemistry B Letters* **2005**, *109*, 9865–9868.

(157) Svensson, E. A.; Delval, C.; von Hessberg, P.; Johnson, M. S.; C Pettersson, J. B. Freezing of Water Droplets Colliding with Kaolinite Particles. *Atmos. Chem. Phys* **2009**, *9*, 4295–4300. https://doi.org/doi.org/10.5194/acp-9-4295-2009.

(158) Ladino, L.; Stetzer, O.; Lüönd, F.; Welti, A.; Lohmann, U. Contact Freezing Experiments of Kaolinite Particles with Cloud Droplets. *Journal of Geophysical Research Atmospheres* **2011**, *116* (22), 1–12. https://doi.org/10.1029/2011JD015727.

(159) Hoffmann, N.; Duft, D.; Kiselev, A.; Leisner, T. Contact Freezing Efficiency of Mineral Dust Aerosols Studied in an Electrodynamic Balance: Quantitative Size and Temperature Dependence for Illite Particles. *Faraday Discuss* **2013**, *165*, 383–390. https://doi.org/10.1039/c3fd00033h.

(160) Nolte, C. G.; Schauer, J. J.; Cass, G. R.; Simoneit, B. R. T. Highly Polar Organic Compounds Present in Wood Smoke and in the Ambient Atmosphere. *Environ Sci Technol* **2001**, *35* (10), 1912–1919. https://doi.org/10.1021/es001420r.

(161) Grieman, M. M.; Aydin, M.; Isaksson, E.; Schwikowski, M.; Saltzman, E. S. Aromatic Acids in an Arctic Ice Core from Svalbard: A Proxy Record of Biomass Burning. *Climate of the Past* **2018**, *14* (5), 637–651. https://doi.org/10.5194/cp-14-637-2018.

(162) Kawamura, K.; Pavuluri, C. M. New Directions: Need for Better Understanding of Plastic Waste Burning as Inferred from High Abundance of Terephthalic Acid in South Asian Aerosols. *Atmos Environ* **2010**, *44* (39), 5320–5321. https://doi.org/10.1016/j.atmosenv.2010.09.016.

(163) Simoneit, B. R. T.; Kobayashi, M.; Mochida, M.; Kawamura, K.; Lee, M.; Lim, H. J.; Turpin, B. J.; Komazaki, Y. Composition and Major Sources of Organic Compounds of Aerosol Particulate Matter Sampled during the ACE-Asia Campaign. *Journal of Geophysical Research D: Atmospheres* **2004**, *109* (19), 1–22. https://doi.org/10.1029/2004JD004598.

(164) Kumar Deshmukh, D.; Mozammel Haque, M.; Kim, Y.; Kawamura, K. Organic Tracers of Fine Aerosol Particles in Central Alaska: Summertime Composition and Sources. *Atmos Chem Phys* **2019**, *19* (22), 14009–14029. https://doi.org/10.5194/acp-19-14009-2019.

(165) Chebbi, A.; Carlier, P. CARBOXYLIC ACIDS IN THE TROPOSPHERE, OCCURRENCE, SOURCES, AND SINKS: A REVIEW. *Atmos Environ* **1996**, *30* (24), 4233–4249.

(166) Kleindienst, T. E.; Jaoui, M.; Lewandowski, M.; Offenberg, J. H.; Docherty, K. S. The Formation of SOA and Chemical Tracer Compounds from the Photooxidation of Naphthalene and Its Methyl Analogs in the Presence and Absence of Nitrogen Oxides. *Atmos Chem Phys* **2012**, *12* (18), 8711–8726. https://doi.org/10.5194/acp-12-8711-2012.

(167) Winterhalter, R.; Kippenberger, M.; Williams, J.; Fries, E.; Sieg, K.; Moortgat, G. K. Concentrations of Higher Dicarboxylic Acids C 5-C 13 in Fresh Snow Samples Collected at the High Alpine Research Station Jungfraujoch during CLACE 5 and 6. *Atmos. Chem. Phys* **2008**, *9*, 2097–2112.

(168) Kavouras, I. G.; Mihalopoulos, N.; Stephanou, E. G. Formation of Atmospheric from Organic Acids by Forests. *Nature* **1998**, *395*, 683–686.

(169) McCluskey, C. S.; Hill, T. C. J.; Sultana, C. M.; Laskina, O.; Trueblood, J.; Santander, M. V; Beall, C. M.; Michaud, J. M.; Kreidenweis, S. M.; Prather, K. A.; et al. A Mesocosm Double Feature: Insights into the Chemical Makeup of Marine Ice Nucleating Particles. *J Atmos Sci* **2018**, *75*, 2405–2423. https://doi.org/10.1175/JAS-D-17.

(170) DeMott, P. J.; Hill, T. C. J.; McCluskey, C. S.; Prather, K. A.; Collins, D. B.; Sullivan, R. C.; Ruppel, M. J.; Mason, R. H.; Irish, V. E.; Lee, T.; et al. Sea Spray Aerosol as a Unique Source of Ice Nucleating Particles. *Proc Natl Acad Sci U S A* **2016**, *113* (21), 5797–5803. https://doi.org/10.1073/pnas.1514034112.